



482  
01/05/2014

UNIVERSITY GRANTS COMMISSIONS - SOUTH EASTERN REGIONAL OFFICE  
5-9-194, CHIRAG ALI LANE, IV FLOOR, A.P.S.F.C. BUILDING, HYDERABAD -500 001  
Phones: 040 - 23204735, 23200208 FAX: 040 - 23204734, Website: [www.ugc.ac.in](http://www.ugc.ac.in), email: [ugcsero@gmail.com](mailto:ugcsero@gmail.com)

No.F MRP-4637/14 (SERO/UGC)

March 2014

The Accounts Officer  
UGC-SERO, Hyderabad

Comcode: APKA018

Category: OBC

**Sub: Release of Grants-in-aid to Minor Research Projects for the year 2013-2014.**  
Sir / Madam,

The has reference to the Minor Research Project proposal submitted by MRS MANASA.G Department of CHEMISTRY of GOVT. DEGREE & P.G COLLEGE FOR WOMEN KASHMIR GADDA KARIMNAGAR entitled "DESIGN,SYNTHESIS AND CHARACTERIZATION OF NEW 1,8-N APHTHYRIDINE SUBSTITUTED HETEROCYCLES AND THEIR BIOLOGICAL EVALUATION". The subject expert, who evaluated the proposal, has recommended for financial assistance as detailed below.

Sl. No	Item	Amount Allocated (Rs.)	Amount Sanctioned as first installment (Rs.)
1.	Books & Journals	15000.	15000.
2.	Equipment	80000.	80000.
	Total	95000.	95000.
3.	Field work & Travel	5000.	2500.
4.	Chemical & Glass Ware	90000.	45000.
5.	Contingency (incl. Special Needs)	10000.	5000.
6.	Hiring Services	0 0	0 0
	Total	105000.	52500.
	Grand Total	200000.	147500.

1. I am further to convey the sanction of the University Grants Commission to the payment of Rs.147500. to the principal, GOVT. DEGREE & P.G COLLEGE FOR WOMEN, KASHMIR GADDA, KARIMNAGAR as first installment (100% Non-Recurring and 50% Recurring grants) towards the above project.

**GRANTS IN AID (31)**

Amount Sanctioned	SC (15%) 2D(i)	ST (7.5%) 2D(ii)	General (77.5%) 5(Viii)
Rs.95000/-	Rs.14250/-	Rs7125/-	Rs.73625.

**CAPITAL (35)**

Amount Sanctioned	SC (15%) 2D(i)	ST (7.5%) 2D(ii)	General (77.5%) 5(Viii)
Rs.52500/-	Rs7875/-	Rs3938/-	Rs.40687/-

2. The above approval is subject to the general conditions of grants prescribed by the UGC for this scheme.
3. The amount of the grant shall be drawn by the Accounts Officer, SERO-UGC, Hyderabad and on the Grants-in-Aid bill and shall be disbursed to and credited to the Principal of the College through Electronic mode. The sanction is valid for payment for the year 2013-2014.
4. In case the Principal investigator is having ongoing Major/Minor Research Project OR has been transferred/left/retired from the college, the released amount may be returned to UGC-SERO, Hyderabad immediately.
5. The grantee institution shall ensure the utilization of grants -in-aid for which it is being sanctioned/paid. in case of non-utilization /part utilization, interest @ 10% per annum as amended from time to time on utilized amount from the date of drawl to the date of refund as per provision contained in General Financial Rules of Govt. of India will be charged.
6. The assets acquired wholly or substantially out of UGC's grants shall not be disposed or encumbered or utilized for the purposes other than those for which the grant was given, without proper sanction of the UGC and should, at any time the college ceased to function, such assets shall revert to the UGC.
7. The Principal investigator of the project is required to submit the First year progress report of the work done along with the documents 1) Annual Report of the Project as per Annexure-III 2) Utilization Certificate

duly signed by the Principal Investigator, Principal & Chartered Accountant 3) Statement of Expenditure for the approved heads for the sanctioned amount as per Annexure-V duly signed by the Principal Investigator, Principal & Chartered Accountant.

8. The interest earned by the College / Institute on this grants-in-aid shall be treated as additional grant which may be shown in the Utilization Certificate / Statement of Expenditure to furnished by the grantee institution.  
MRP-4637/14
9. The college has to send the filled in Acceptance certificate within 15 days of receipt of this letter, else the college may return back the sanctioned amount to this office. Further if the conditions of the acceptance letter is not acceptable or applicable to the P.I/College, the sanctioned amount be refunded back to SERO-UGC, Hyderabad.
13. The guidelines of Minor Research Project have to be followed in toto.
14. The Grant is subject to the adjustment on the basis of Utilization Certificate I the prescribed proforma submitted by the University/Institution.
15. The University/Institution shall maintain proper accounts of the expenditure out of the Grants, which shall be utilized, only on the approved items of expenditure.
16. The Utilization Certificate to the effect that the grant has been utilized for the purpose for which it has been sanctioned shall be furnished to UGC as early as possible after the close of current financial year.
17. The college shall maintain a Register of Assets acquired wholly or substantially out of the grant in the prescribed proforma.
18. The College shall fully implement to Official languages Policy of Union Govt. and comply with the Official Language Act, 1963 and Official languages (use for official purposes of the Union) Rules, 1976 etc.,
19. The sanction issues in exercise of the delegation of powers vide Commission Office Order No. 130/2013 [F.No: 10—11/12 (Admn./ A& B) Dated 28.05.2013.

Yours faithfully,

(Dr.G.Srinivas)  
Joint Secretary

Copy to:

1. ✓ The Principal (Along with DD / Funds transferred through E-mode)  
GOVT. DEGREE & P.G COLLEGE FOR WOMEN  
KASHMIR GADDA, KARIMNAGAR -505001
2. MRS. MANASA.G  
Dept. of CHEMISTRY  
GOVT. DEGREE & P.G COLLEGE FOR WOMEN  
KASHMIR GADDA, KARIMNAGAR -505001
3. The Dean/Director, College Development Council of affiliating University
4. The Commissioner /Director Collegiate Education, Government of ANDHRA PRADESH
5. The Principal Accounts General (A & E)- Government of ANDHRA PRADESH

(Yamsika C)  
Education Officer

Gar Cap.SI.No.212./2013-2014 Gar GIA SI.No.345./2013-2014

Details of Payment by RTGS/NEFT to the College

The sanctioned grant of Rs. 147500. has been transferred to your college Account No 040501000016201 at Bank IOB, KARIMNAGAR with IFS Code: IOBA0000405 through RTGS/Direct Credit (CBS to CBS). The Canara Bank, Abids, Hyderabad (CNRB 000 0606) has confirmed the above transfer of funds to your college through RTGS/Direct Credit transaction vide UTR confirmation

No. P14040882405541 Dated 08/04/14

Your are requested to confirm the receipt of the above amount in your account by sending back the enclosed stamped receipt with in 7 days.

(R.Rayappa)  
Accounts Officer

PG- 70/13-14

106



No.SB/EMEQ-283/2014

**विज्ञान और इंजीनियरिंग अनुसंधान बोर्ड (एसईआरबी)**

(विज्ञान और प्रौद्योगिकी विभाग, भारत सरकार के एक सांविधिक निकाय)

**Science and Engineering Research Board (SERB)**

(A Statutory body under Department of Science & Technology, Govt. of India)

5 & 5A, Lower Ground Floor,  
Vasant Square Mall, Plot No. A,  
Community Centre, Sector-B, Pocket-5  
Vasant Kunj, New Delhi-110070

Date: 08-08-2017

**ORDER**

**Sub:** Research project entitled, "*The development of cost effective solid adsorbents for CO2 capture*" under the guidance of **Ms. J Madhavi, Department of Chemistry, Govt. Degree College for Women, Kashmirgadda, , Karimnagar-505001, Andhra Pradesh – Release of grant.**

In continuation to SERB's sanction order No. " **SB/EMEQ-283/2014** dated 09.03.2016" sanction of the **Science & Engineering Research Board (SERB)** is here by accorded to the payment of a sum of **Rs.4,00,000/- (Rupees four lakh only)** as the grant for the financial year(FY) 2017-2018 for implementation of the above said project.

2. Sanction of the Competent authority is also accorded to carry forward the remaining unspent balance of **Rs.59,006/-** from the FY 2016-17 to **CFY 2017-18** for utilization of the same purpose for which it was sanctioned.

3. Sanction of the grant is subject to the conditions as detailed in Terms & Conditions available at website ([www.serb.gov.in](http://www.serb.gov.in)).

4. It is certified that provisions of GFR 212 relating to Utilization Certificates (UCs) for the funds released under the grant have been satisfied and the UC is enclosed herewith.

5. The expenditure involved is debitable to "**Fund for Science & Engineering Research (FSER/SC) – Recurring Head**". This release is made under "**Empowerment and Equity Opportunities for Excellence in Science**" program.

6. The Sanction has been issued with the approval of the competent authority under delegated powers and vide Diary No. **SERB/F/4433/2017-18** dated 05-08-2017.

7. The amount of **Rs.4,00,000/- (Rupees four lakh only)** will be drawn by the Finance & Budget Officer of the SERB and will be disbursed by means of RTGS transaction as per their Bank details given below

<b>Account Name</b>	<b>Principal, Govt Degree College Women, Karimnagar</b>
<b>Account Number</b>	<b>040501000016201</b>
<b>Bank Name &amp; Branch</b>	<b>Indian Bank, Karimnagar</b>
<b>IFSC/RTGS Code</b>	<b>IOBA 0000405</b>

8. The Institute will maintain separate audited accounts for the Project. It is found expedient to keep a part or whole of the grant in a bank account earning interest. The interest earned should be reported to the SERB. The interest thus earned will be treated as a credit to the institute to be adjusted towards further installment of the grant.

Cont...2/-

9. As per rule 211 of GFR the accounts of Grantee Institution shall be open to inspection by the sanctioning authority / audit whenever the institute is called upon to do so.
10. The Institute will furnish to the SERB, Utilization Certificate and an Audited Statement of Account pertaining to the grant immediately after the end of each financial year.
11. After completion of the project unspent balance if any should be returned as Demand Draft drawn in favor of "**Fund for Science and Engineering Research**" payable at New Delhi.
12. The organization/institute/university should ensure that the technical support/financial assistance provided to them by the Science & Engineering Research Board, a statutory body of the Department of Science & Technology (DST), Government of India should invariably be highlighted/acknowledged in their media releases as well as in bold letters in the opening paragraphs of their Annual Report.
13. In addition, the investigator/ host institute must also acknowledge the support provided to them in all publications, patents and any other output emanating out of the project/ program funded by the Science & Engineering Research Board, a statutory body of the Department of Science & Technology (DST), Government of India.



डॉ प्रमोद कुमार प्रसाद/ वैज्ञानिक सी  
Dr. Pramod Kumar Prasad/SCIENTIST-C

To,

**Finance & Budget Officer**  
**SERB, New Delhi**

**Copy forwarded for information and necessary action to: -**

1. The Principal Director of Audit, A.G.C.R. Building, III<sup>rd</sup> Floor I.P. Estate, Delhi-110002.
2. Sanction Folder, SERB, New Delhi.
3. File Copy
4. **Ms.J Madhavi**  
**Department of Chemistry**  
**Govt. Degree College for Women**  
**Kashmirgadda, ,**  
**Karimnagar – 505001**  
**E-Mail: madhavi0521@gmail.com,**
5. **The Director**  
**Govt. Degree College for Women**  
**Kashmirgadda,**  
**Karimnagar – 505001**



डॉ प्रमोद कुमार प्रसाद/ वैज्ञानिक सी  
Dr. Pramod Kumar Prasad/SCIENTIST-C

SB/EMEQ-283/2014

SCIENCE & ENGINEERING RESEARCH BOARD

5 & 5A, Lower Ground Floor,  
Vasant Square Mall, Plot No. A,  
Community Centre, Sector-B, Pocket-5  
Vasant Kunj, New Delhi-110070

Dated 9/3/2016

ORDER

**Subject:** Financial Sanction of the research project titled "*The development of cost effective solid adsorbents for CO2 capture*", under the guidance of Dr. J Madhavi, Department of Chemistry, Govt. Degree College for Women, Karimnagar-505001, Andhra Pradesh.

Sanction of Science and Engineering Research Board (SERB) is hereby accorded to the above mentioned project at a total cost of Rs.11,00,000/- (Rupees Eleven lakh only) under Recurring head for a duration of 2 years. The items of expenditure for which the total allocation of Rs.11,00,000/- has been approved for a period of 2 years, are given below:

1	Head	Total (in Rs.)
	Recurring Items (General)	
1.	General -A Manpower, Consumables, National Travel, Contingencies and Minor Equipments.	10,00,000/-
2.	General -B Overhead Charges	1,00,000/-
	Total (General-A + General-B)	11,00,000/-

- Sanction of the SERB is also accorded to the payment of Rs.6,00,000/- (Rupees Six lakhs only) under "Recurring" being the grant for the year 2015-16, for implementation of the above said research project.
- The expenditure involved is debit to "Fund for Science & Engineering Research (FSER-SC)". This release is made under "Empowerment and Equity Opportunities for Excellence in Science" program.
- The Sanction has been issued with approval of the competent authority under delegated powers and vide Diary No, SERB/F/8156/2015-16 dated 03.03.2016.
- Sanction of the grant is subject to the condition given at the website [www.serb.gov.in](http://www.serb.gov.in).
- Overhead expenses are meant for the host Institute towards the cost for providing infrastructural facilities and general administrative support etc. including benefits to the staff employed in the project.
- While providing operational flexibility among various subheads under head General-A, it should be ensured that not more than Rs.75,000/- each should be spent for travel and contingency.

Cont.2/-

8. The total release amount of **Rs.6,00,000/- (Rupees six lakhs only)** will be drawn by the **Finance and Budget Officer of the SERB** and will be disbursed by means of RTGS transaction as per their Bank details given below

Account Name	PRINCIPAL, GOVT.DEGREE COLLEGE WOMEN, KARIMNAGAR
Account Number	040501000016201
Bank Name & Branch	INDIAN OVERSEAS BANK, KARIMNAGAR
IFSC/RTGS Code	IOBA0000405

9. The institute will maintain separate audited accounts for the project. It is found expedient to keep a part or whole of grant in a bank account earning interest, the interest earned should be reported to the SERB, New Delhi. The interest thus earned will be treated as a credit to the institute to be adjusted towards further installment of the grant.

10. As per rule 211 of GFRs, the accounts of project shall be open to inspection by sanctioning authority/audit whenever the institute is called upon to do so.

11. The institute will furnish to the SERB, Utilization Certificate and an Audited statement of accounts pertaining to the grant immediately after the end of each financial year.

12. The manpower sanctioned in the project, if any is co-terminus with the duration of the project and SERB will have no liability to meet the fellowship etc. beyond the duration of the project

13. The sanctioned equipments and consumbles would be procured as per GFR 2005 and its disposal would be done with prior approval of SERB.

14. As this is the first grant being released for the project, no previous U/C is required.

15. After completion of the project unspent balance, if any, should be returned as Demand Draft drawn in favor of "**Fund for Science and Engineering Research**" payable at New Delhi.



(AMITAVA ROY)  
SCIENTIST-F

To,  
Finance & Budget Officer  
SERB, New Delhi.

Copy forwarded for information and necessary action to: -

1. The Principal Director of Audit, A.G.C.R. Building, III<sup>rd</sup> Floor I.P. Estate, Delhi-110002.
2. Sanction folder, SERB, New Delhi.
3. File Copy
4. **Dr. J Madhavi**  
Department of Chemistry  
Govt. Degree College for Women  
Karimnagar-505001, Andhra Pradesh.  
Email id: madhavi0521@gmail.com
5. **The Principal**  
Govt. Degree College for Women  
Karimnagar-505001, Andhra Pradesh.



(AMITAVA ROY)  
SCIENTIST-F

## Mesoporous carbon supported MgO for CO<sub>2</sub> capture and separation of CO<sub>2</sub>/N<sub>2</sub>

Harshitha Burri\*, Rumana Anjum\*, Ramesh Babu Gurrum\*\*, Harisekhar Mitta\*\*\*, Suresh Mutyala\*\*\*\*, and Madhavi Jonnalagadda\*<sup>†</sup>

\*Department of Chemistry, Government Degree College for Women, Karimnagar, Telangana, India

\*\*Catalysis Laboratory, Indian Institute of Chemical Technology, Hyderabad-500007, India

\*\*\*State Key Laboratory of Catalysis, Dalian Institute of Chemical Physics, Chinese Academy of Science, Dalian-116023, China

\*\*\*\*Department of Chemistry and Key Laboratory for Preparation and Application of Ordered Structural Materials of Guangdong Province, Shantou University, Guangdong 515063, China

(Received 3 February 2019 • accepted 23 July 2019)

**Abstract**—Mesoporous carbon derived from pongamia pinnata fruit hulls was used as support to incorporate magnesium oxide for the study of CO<sub>2</sub> adsorption and separation of CO<sub>2</sub>/N<sub>2</sub>. All synthesized adsorbents were characterized by PXRD, N<sub>2</sub> adsorption-desorption isotherms, Raman and SEM with EDX techniques. Characterization results revealed the existence of magnesium oxide on mesoporous carbon. CO<sub>2</sub> adsorption on MgO incorporated mesoporous carbon was higher than bulk mesoporous carbon, due to the electrostatic interaction between magnesium oxide and CO<sub>2</sub>. High CO<sub>2</sub> adsorption capacity 1.68 mmol/g was obtained for 10 wt% MgO incorporated mesoporous carbon at 298 K, 1 bar compared to remaining loadings, because of the high content of MgO. However, the N<sub>2</sub> adsorption capacity decreased with the increase of MgO content due to a decrease in surface area and no interaction of the N<sub>2</sub> molecule with the adsorbent. The selectivity of CO<sub>2</sub>/N<sub>2</sub> was higher on 10 wt% MgO incorporated mesoporous carbon and the value was 40. The heat of CO<sub>2</sub> adsorption was 36 KJ/mol at low coverage of CO<sub>2</sub>, and CO<sub>2</sub> adsorption capacity was constant in each adsorption cycle over the same adsorbent.

Keywords: MgO, Mesoporous Carbon, CO<sub>2</sub> and N<sub>2</sub> Adsorption, Selectivity, Heat of CO<sub>2</sub> Adsorption

### INTRODUCTION

Carbon dioxide is one of the environmental pollutant gases causing global warming. It is produced by the consumption of fossil fuel, high growth of petrochemical, automobile industries, and power plants [1]. CO<sub>2</sub> concentration can be minimized by the development of an alternative energy source until commercial energy sources have to use for the production of energy. Carbon dioxide in the atmosphere can be reduced by carbon capture and separation. In power plants, a large amount of CO<sub>2</sub> is liberated that is absorbed by the use of liquid amine solutions. However, a large amount of energy is required for the regeneration, and volatile organic compounds are liberated which damage the pipeline system [2]. Adsorption is one of the best techniques to reduce the concentration of CO<sub>2</sub>. In this process, energy consumption and damage to the pipeline system are less. So far, commercially available carbon materials [3], zeolites [4], clays [5] and silica materials [6] have been used for CO<sub>2</sub> capture and separation.

Activated carbon is one of the most abundant carbon materials [7]. However, large-scale synthesis is hindered because of the non-renewable source. Porous carbon was synthesized from renewable sources such as waste tea [8], coffee grounds [9], cotton stalk [10],

peach stone and olive stone [11,12], biodiesel solid residue [13] and rice husk [14]. Pongamia pinnata fruit hulls are also a source for the porous carbon synthesis. Bio-oil is produced from pongamia pinnata seeds. During the production of bio-oil, pongamia pinnata fruit hulls are thrown without any commercial use. From the fruit hulls, we have synthesized mesoporous carbon to capture CO<sub>2</sub>. CO<sub>2</sub> adsorption capacity on mesoporous carbon can be enhanced by the incorporation of basic metal oxides, amine or heteroatom which generates basic sites to capture CO<sub>2</sub>.

Iron oxide-doped MCM-41 has shown CO<sub>2</sub> adsorption capacity 0.87 mmol/g at 298 K, 1 bar [15]. CeO<sub>2</sub> incorporated mesoporous carbon showed CO<sub>2</sub> adsorption 1.77 mmol/g at 303 K, 1 bar [16]. Cu<sub>2</sub>O and NiO incorporated porous carbon showed high CO<sub>2</sub> adsorption capacity compared to bulk porous carbon [17,18]. S-doped microporous carbon has shown 3.7 mmol/g of CO<sub>2</sub> adsorption at 298 K, 1 bar [19]. N-enriched activated carbon from Procamburus Clarkii shells has shown 2.55 mmol/g of CO<sub>2</sub> adsorption at 298 K, 1 bar [20]. MgO modified mesoporous silica has shown 1.34 mmol/g of CO<sub>2</sub> at 303 K [21]. Similarly, MgO supported titanium oxide showed 0.48 mmol/g of CO<sub>2</sub> adsorption at 298 K [22]. In all reported adsorbents, the CO<sub>2</sub> adsorption capacity was higher due to electrostatic interaction between a metal oxide and CO<sub>2</sub>. In this article, we studied CO<sub>2</sub> adsorption on mesoporous carbon and magnesium oxide incorporated mesoporous carbon in low pressure at 298 K. Moreover, the selectivity of CO<sub>2</sub>/N<sub>2</sub>, the heat of CO<sub>2</sub> adsorption and multiple CO<sub>2</sub> adsorption cycles was studied.

<sup>†</sup>To whom correspondence should be addressed.

E-mail: madhavi0521@gmail.com

Copyright by The Korean Institute of Chemical Engineers.

## EXPERIMENTAL

### 1. Materials

All analytical grade chemicals such as magnesium nitrate hexahydrate (Mg(NO<sub>3</sub>)<sub>2</sub>·6H<sub>2</sub>O), Orthophosphoric acid (H<sub>3</sub>PO<sub>4</sub>) were purchased from all commercial sources and used without further purification. Laboratory purified double distilled water was used for the synthesis of adsorbents. Ultra-high pure gases such as helium, carbon dioxide, nitrogen were purchased from local suppliers in India.

### 2. Synthesis of Adsorbents

Pongamia pinnata fruit hulls were collected from the forest region of Telangana, India. The fruit hulls were dried and crushed into a fine powder, then chemically activated using orthophosphoric acid with 1:1 (w/w%) followed by drying at 100 °C for 12 h, then calcined at 723 K for 4 h in a nitrogen atmosphere. The obtained product was washed with distilled water until neutral pH was obtained, then vacuum dried at 373 K for 12 h. Finally, we got mesoporous carbon [23]; it was denoted as MC. Magnesium oxide incorporated mesoporous carbon was synthesized by the impregnation method. The desired quantity of magnesium nitrate hexahydrate was dissolved in 10 mL distilled water, then 1 g of mesoporous carbon was added to it. The mixture was stirred at room temperature for 1 h, then dried at 373 K for 12 h. The dried product was calcined at 723 K for 4 h in the nitrogen atmosphere. Finally, we got magnesium oxide incorporated mesoporous carbon; it was denoted as xMgO/MC, where x represents the weight percentage of magnesium oxide (x=2, 5 and 10).

### 3. Characterization

Powdered X-ray diffraction patterns were recorded on Rigaku MiniFlex600 X-ray diffractometer using Ni-filtered Cu K<sub>α</sub> radiation ( $\lambda=1.54 \text{ \AA}$ ) in the scan range  $2\theta=10\text{--}80^\circ$ . N<sub>2</sub> adsorption-desorption isotherms were measured using Micromeritics ASAP 2020 surface area and porosity analyzer at 77 K. Prior to adsorption study, about 0.1 g of sample was degasified at 473 K for 4 h under vacuum. The specific surface area was calculated by the BET method. Total pore volume at a relative pressure of 0.99 and micropore volume by the t-plot method was calculated from N<sub>2</sub> adsorption-desorption isotherms. Raman spectra were recorded using LabRAM HR800 Raman spectrometer having laser wavelength 514 nm. Morphological image with metal composition was obtained from ZEISS Sigma 300 Scanning electron microscope analyzer.

### 4. CO<sub>2</sub> and N<sub>2</sub> Adsorption Measurement

CO<sub>2</sub> and N<sub>2</sub> adsorption isotherms were measured on Micromeritics ASAP 2020 analyzer at low pressure 0-100 kPa at 298 K. Sample temperature was controlled by the thermostatic bath which was connected to water circulating jacket. Free space of the sample was measured using helium gas. About 0.1 g of sample was degasified similar to N<sub>2</sub> adsorption-desorption isotherm measurement at 77 K, then cooled to room temperature for the study of CO<sub>2</sub> and N<sub>2</sub> adsorption isotherms. The selectivity of CO<sub>2</sub>/N<sub>2</sub> was calculated using the initial slope of each isotherm by Henry's Law. The heat of CO<sub>2</sub> adsorption was calculated by the Clausius-Clapeyron equation using adsorption isotherms measured at 283, 298 and 303 K. Multiple CO<sub>2</sub> adsorption cycles were also carried out, after desorbing adsorbed CO<sub>2</sub> at 473 K for 2 h under vacuum.

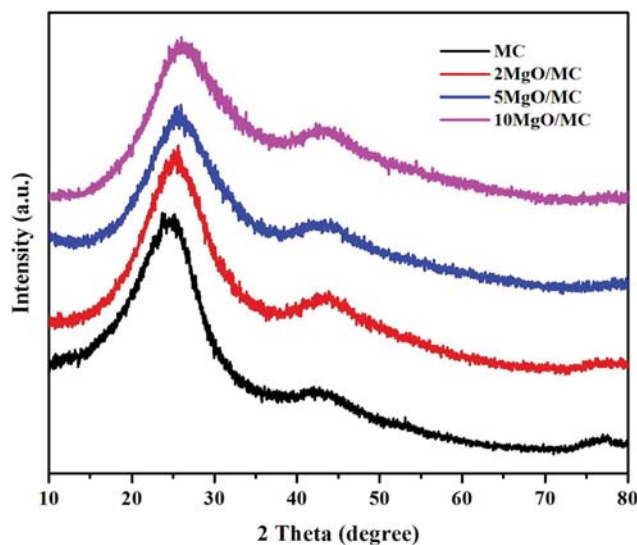


Fig. 1. XRD patterns of MC and MgO incorporated MC.

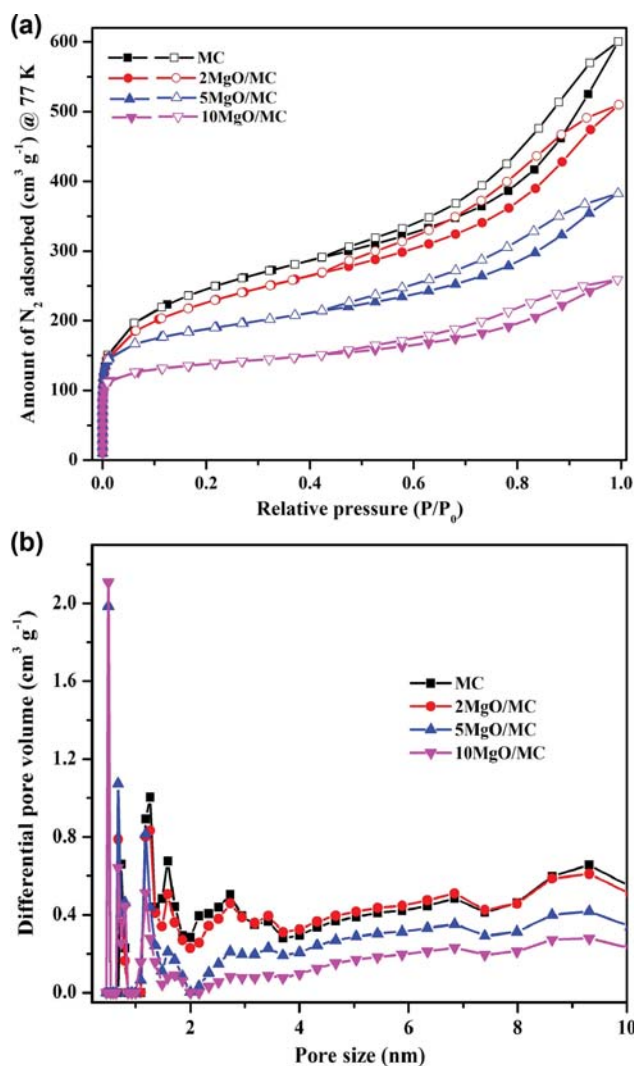


Fig. 2. (a) N<sub>2</sub> adsorption-desorption isotherms and (b) pore size distribution of MC and MgO incorporated MC.



## RESULTS AND DISCUSSION

The X-ray diffraction pattern of mesoporous carbon and MgO incorporated mesoporous carbon samples are shown in Fig. 1. MC shows two broad diffraction peaks at  $2\theta=24.2^\circ$  and  $43.66^\circ$  having planes (002) and (100), respectively, which are characteristic peaks of mesoporous carbon [24]. Moreover, MgO incorporated mesoporous carbon samples also show diffraction peaks similar to mesoporous carbon and no diffraction peaks related to MgO appeared. It indicates that MgO was well-dispersed over mesoporous carbon. However, the intensity of major diffraction peaks of MC decreased with the increase of MgO loading and shifted towards higher angle. Similar results have been reported on nickel loaded MCM-41 for hydrogen storage [25].

From  $N_2$  adsorption-desorption isotherm, the porosity of carbon material can be found. Fig. 2 shows  $N_2$  adsorption-desorption isotherms of MC and MgO incorporated MC at 77 K. Textural properties are presented in Table 1. MC shows a large amount of  $N_2$  uptake below the relative pressure of 0.1 and a hysteresis loop above the relative pressure of 0.4. The isotherm pattern of MC is similar to type-I and type-IV of classification of porous materials by IUPAC [26], which represent that MC has micro and mesopores. The specific surface area, total pore volume and pore size of MC were  $840\text{ m}^2/\text{g}$ ,  $0.94\text{ cm}^3/\text{g}$ , and  $4.4\text{ nm}$ , respectively. Similarly, MgO incorporated MC samples show the same isotherm pattern similar to MC. But, the amount of  $N_2$  uptake is less. As the content of MgO increased, the amount of  $N_2$  uptake was decreased. Hence, a change in textural properties has been observed. The specific surface area was decreased to  $421\text{ m}^2/\text{g}$ , the total pore volume  $0.34\text{ cm}^3/\text{g}$  and pore size  $3.8\text{ nm}$ . However, micropore surface area and micropore volume were increased, which indicates that incorporated MgO has occupied mesopores of MC.

Raman analysis is used to determine the crystallinity of carbon material. Fig. 3 shows the Raman spectra of MC and 10MgO/MC. Mesoporous carbon shows two Raman bands at  $1,325\text{ cm}^{-1}$  and  $1,580\text{ cm}^{-1}$  which correspond to D-band and G-band, respectively [27]. D-band represents disordered carbon and G-band represents graphitic carbon. The ratio of the intensity of bands ( $I_D/I_G$ ) represents the degree of graphitization. In mesoporous carbon, the intensity of G-band is higher than D-band. It represents that mesoporous

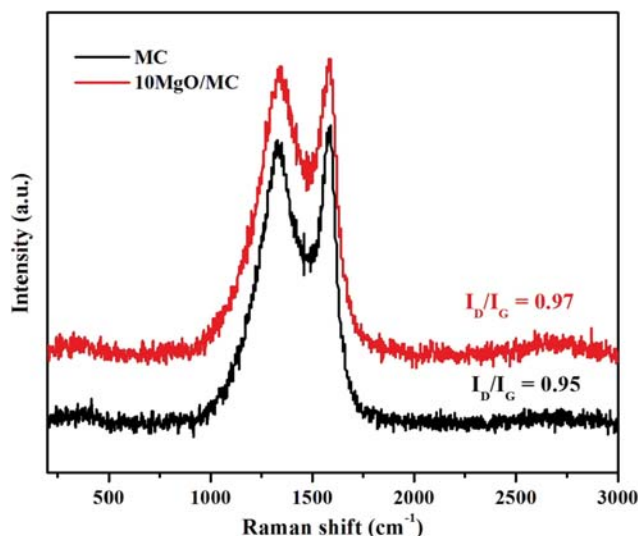


Fig. 3. Raman spectra of MC and MgO incorporated MC.

carbon has a graphitic nature. The  $I_D/I_G$  value was 0.95 for MC and 0.97 for 10MgO/MC. By incorporation of MgO, the graphitic nature of MC decreased [28]. Morphology with the elemental composition of MC and 10MgO/MC is shown in Fig. 4. MC shows irregular shaped carbon particles (Fig. 4(a)). Same morphology was replicated in 10 wt% MgO incorporated mesoporous carbon, which indicates that magnesium oxide was homogeneously distributed over carbon surface (Fig. 4(b)). The amount of magnesium was calculated from EDX and the value was 4.92 wt%.

Fig. 5(a) shows single component adsorption isotherm of  $CO_2$  on MC and MgO incorporated MC samples in low pressure at 298 K. With the increase of  $CO_2$  pressure, the amount of  $CO_2$  adsorption capacity was increased.  $CO_2$  adsorption capacity was  $0.9\text{ mmol g}^{-1}$  for MC,  $1.0\text{ mmol g}^{-1}$  for 2MgO/MC,  $1.5\text{ mmol g}^{-1}$  for 5MgO/MC and  $1.68\text{ mmol g}^{-1}$  for 10MgO/MC at 298 K, 1 bar. The  $CO_2$  adsorption capacity of MgO incorporated MC samples was higher compared to MC because of electrostatic interaction between MgO and  $CO_2$ . With the increase of MgO content, the amount of  $CO_2$  adsorption capacity increased due to the high content of magnesium oxide. It could be confirmed by calculating the amount of

Table 1. Textural properties of MC and MgO incorporated MC

Adsorbent	$S_{BET}^a$ ( $\text{m}^2\text{ g}^{-1}$ )	$S_{micro}^b$ ( $\text{m}^2\text{ g}^{-1}$ )	$V_{total}^c$ ( $\text{cm}^3\text{ g}^{-1}$ )	$V_{micro}^d$ ( $\text{cm}^3\text{ g}^{-1}$ )	$V_{meso}^e$ ( $\text{cm}^3\text{ g}^{-1}$ )	$V_{meso}^f$ (%)	Pore size <sup>g</sup> (nm)
MC	840	225	0.93	0.11	0.82	88	4.4
2MgO/MC	743	189	0.79	0.11	0.68	86	4.2
5MgO/MC	591	293	0.59	0.16	0.43	73	4.0
10MgO/MC	421	263	0.40	0.14	0.26	65	3.8

<sup>a</sup>Multipoint BET surface area

<sup>b</sup>Micropore surface area by t-plot

<sup>c</sup>Total pore volume at  $P/P_0=0.99$

<sup>d</sup>Micropore volume by t-plot

<sup>e</sup>Mesopore volume =  $V_{total} - V_{micro}$

<sup>f</sup>Mesopore volume (%) =  $V_{meso}/V_{total}$

<sup>g</sup>Average pore size by BET method ( $4V/S.A$ )

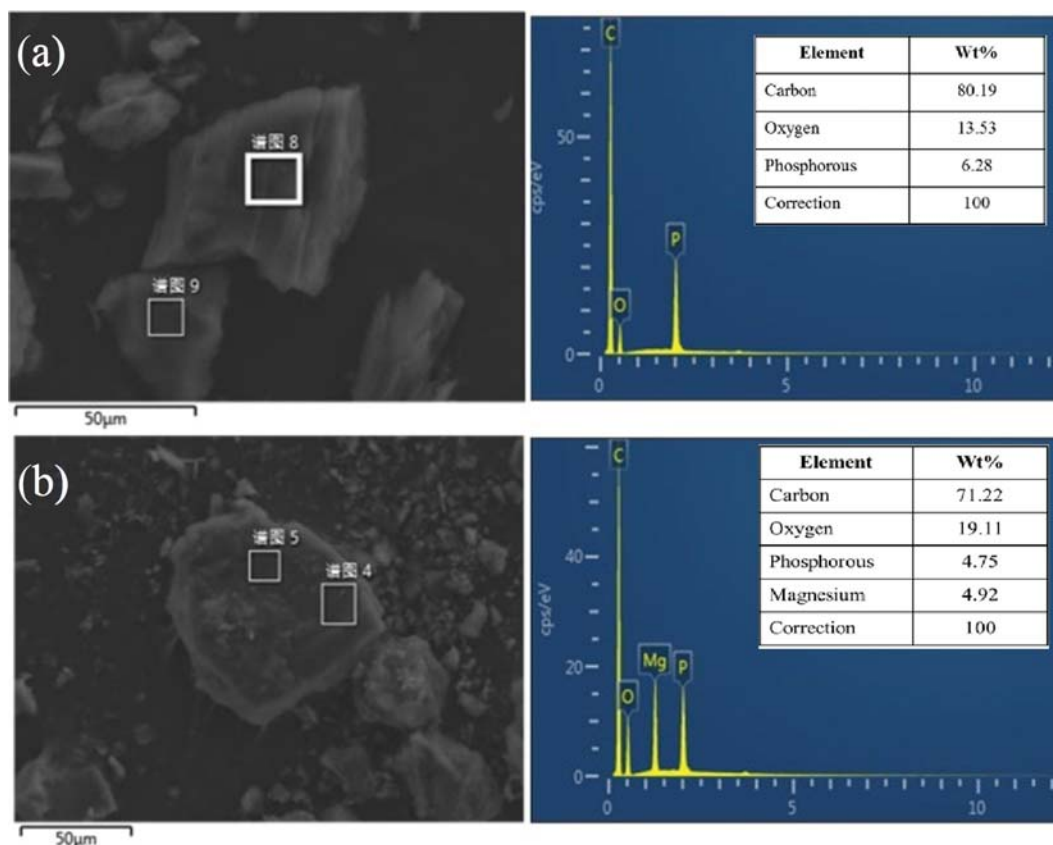


Fig. 4. SEM with EDX of (a) MC and (b) 10MgO/MC.

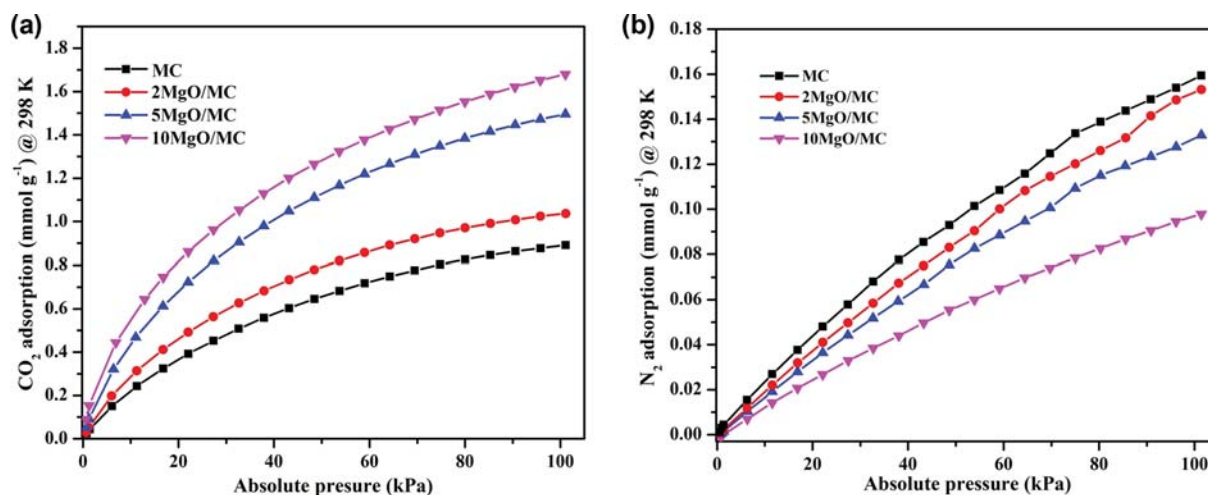


Fig. 5. (a) CO<sub>2</sub> and (b) N<sub>2</sub> adsorption isotherms of MC and MgO incorporated MC at 298 K.

CO<sub>2</sub> adsorption on unit surface area (Fig. 6(a)). CO<sub>2</sub> adsorption on the unit surface area of MgO incorporated mesoporous carbon samples was higher than porous carbon. Hence, CO<sub>2</sub> adsorption depends on the surface chemistry of the adsorbent instead of surface area. Fig. 5(b) shows N<sub>2</sub> adsorption of synthesized adsorbents under a similar condition of CO<sub>2</sub> adsorption. The N<sub>2</sub> adsorption capacity was 0.16 mmol g<sup>-1</sup> for MC, 0.15 mmol g<sup>-1</sup> for 2MgO/MC, 0.13 mmol g<sup>-1</sup> for 5MgO/MC and 0.09 mmol g<sup>-1</sup> for

10MgO/MC at 298 K, 1 bar. The decrease in N<sub>2</sub> adsorption capacity with the increase of MgO content was due to the decrease in surface area.

The difference in adsorption capacity of CO<sub>2</sub> and N<sub>2</sub> is helpful for studying the selectivity of CO<sub>2</sub> over N<sub>2</sub>. In industrial flue gas, CO<sub>2</sub> is a major component gas, so it is essential to study the selectivity of CO<sub>2</sub>/N<sub>2</sub>. It was calculated using the initial slope of each isotherm in low pressure by Henry's law [29]. Fig. 6(b) shows the

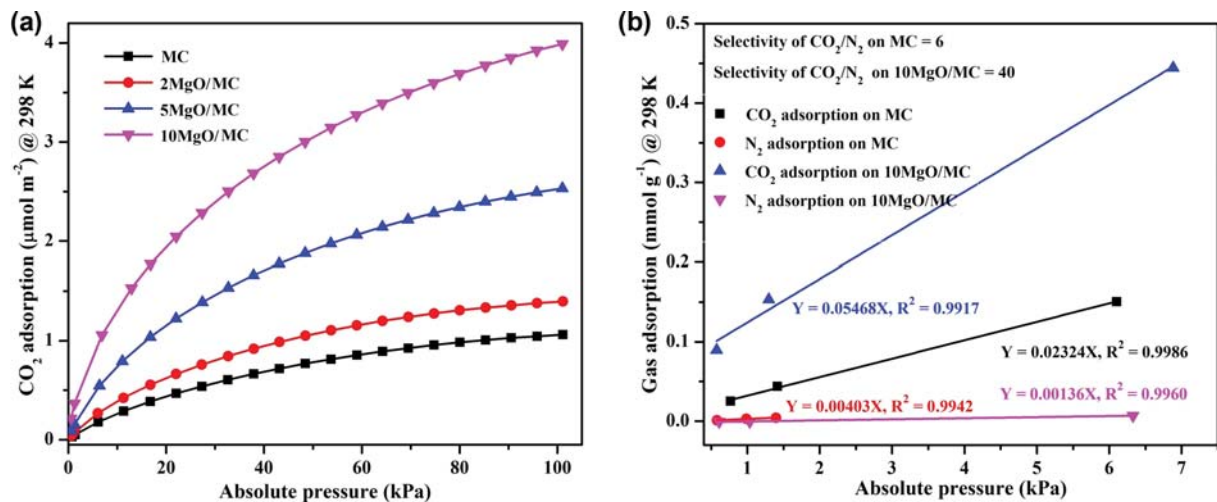


Fig. 6. (a) CO<sub>2</sub> adsorption on unit surface area, (b) selectivity of CO<sub>2</sub>/N<sub>2</sub> on MC and 10MgO/MC.

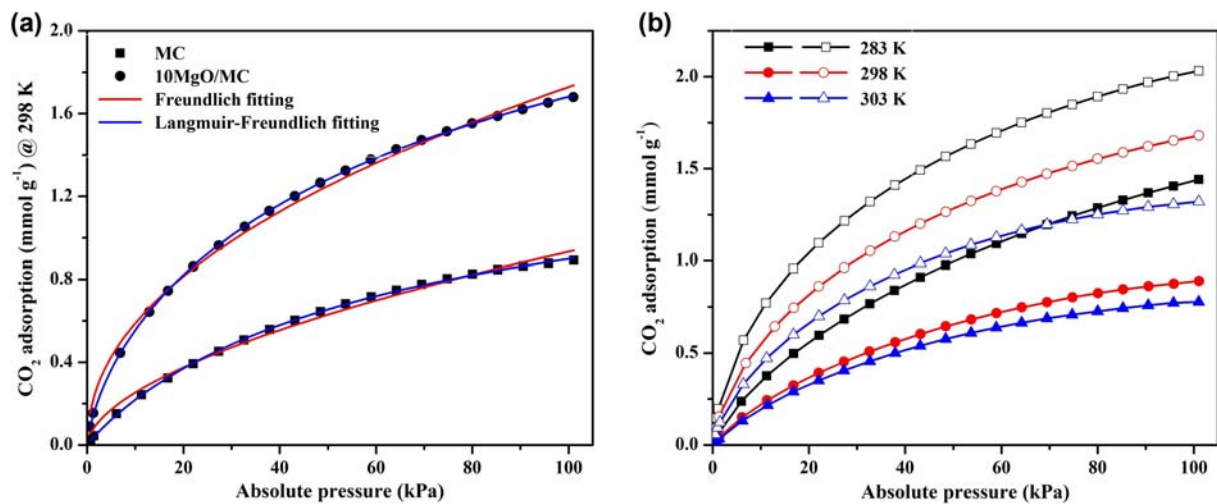


Fig. 7. (a) Fitting curves of experimental CO<sub>2</sub> adsorption data (b) CO<sub>2</sub> adsorption of MC (closed symbol) and 10MgO/MC (open symbol) at different temperatures.

Table 2. Fitting parameters of Freundlich and Langmuir-Freundlich models

Adsorbent	Freundlich model			Langmuir-Freundlich model			
	$k_F$ (kPa <sup>-1</sup> )	$n$	$R^2$	$Q_{max}$ (mmol g <sup>-1</sup> )	$K$ (kPa <sup>-1</sup> )	$n$	$R^2$
MC	0.0688	1.7666	0.9909	1.4988	0.0195	1.0609	0.9997
10MgO/MC	0.2005	2.1378	0.9942	3.2968	0.0395	1.4077	0.9999

selectivity of CO<sub>2</sub>/N<sub>2</sub> on MC and 10MgO/MC. The selectivity value was 6 for MC and 40 for 10MgO/MC. High selectivity value on 10MgO/MC was due to the high adsorption of CO<sub>2</sub>. To describe the adsorption of CO<sub>2</sub> on the adsorbent, experimental CO<sub>2</sub> adsorption data of all synthesized adsorbents was fitted with Freundlich and Langmuir-Freundlich models [30]. These models can be expressed as follows.

$$\text{Freundlich model: } Q = k_F P^{1/n} \quad (1)$$

$$\text{Langmuir-Freundlich model: } Q = Q_{max} \frac{KP^{1/n}}{1 + KP^{1/n}} \quad (2)$$

where  $Q$  is adsorption capacity at equilibrium in mmol/g,  $Q_{max}$  is maximum adsorption capacity in mmol/g,  $P$  is pressure in kPa,  $k_F$  and  $K$  are Freundlich, Langmuir-Freundlich coefficients and  $n$  is heterogeneity factor. Fitting curves of experimental CO<sub>2</sub> adsorption data of MC and 10MgO/MC are shown in Fig. 7(a) and fitting parameters are presented in Table 2. Langmuir-Freundlich model was well-fitted with experimental CO<sub>2</sub> adsorption data of both adsorbents with regression coefficient ( $R^2$ ) higher than 0.999, and  $Q_{max}$  was higher on 10MgO/MC.

The interaction between adsorbent and adsorbate can be known by calculating the heat of adsorption using the Clausius-Clapeyron

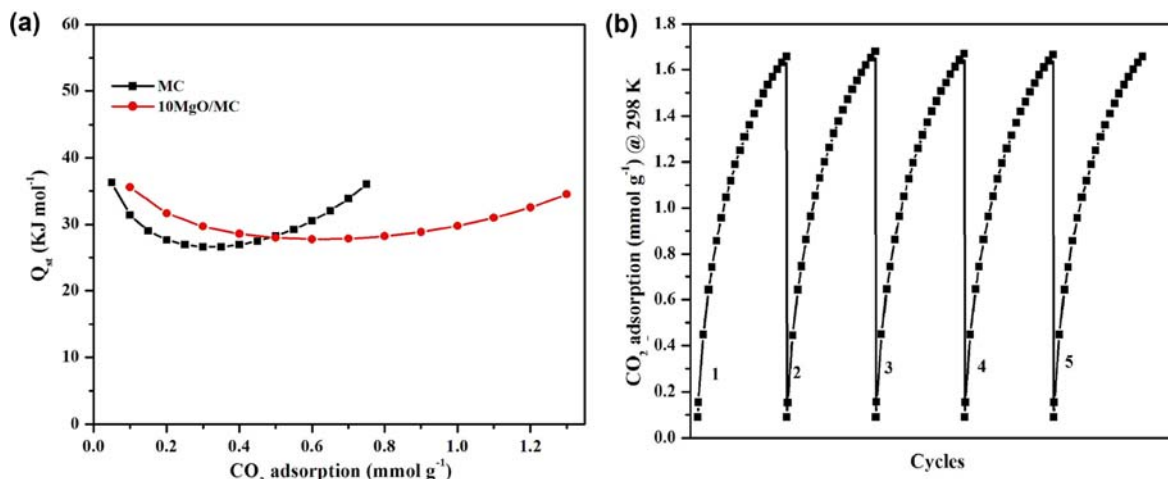


Fig. 8. (a) Heat of CO<sub>2</sub> adsorption on MC and 10MgO/MC, (b) CO<sub>2</sub> adsorption cycles of 10MgO/MC at 298 K.

Table 3. Comparison of CO<sub>2</sub> adsorption capacity and selectivity with reported adsorbents

Adsorbent	CO <sub>2</sub> adsorption at 298 K, 1 bar ( $\text{mmol g}^{-1}$ )	Selectivity (CO <sub>2</sub> /N <sub>2</sub> )	Reference
NiO/mesoporous carbon	2.02 (303 K)	17.6	[16]
Fe <sub>2</sub> O <sub>3</sub> doped MCM-41	0.87	-	[15]
Zeolite-13X	1.70	-	[32]
Karanja seed cake	1.78 (343 K)	-	[33]
MgO/Al <sub>2</sub> O <sub>3</sub>	1.60 (333 K)	-	[34]
N-doped microporous carbon	1.9	21	[29]
MgO/mesoporous carbon	1.68	40	Present work

equation [31]:

$$\ln P = \frac{-Q_{st}}{RT} + C$$

Here, P is pressure in kPa, T is the absolute temperature in K, R is universal gas constant (8.314 J/K·mol), C is constant and  $Q_{st}$  is the heat of adsorption. The partial pressure at different temperatures for the fixed amount of gas uptake can be obtained from the Langmuir-Freundlich model. By drawing a graph between  $\ln P$  versus  $1/T$  with straight line fitting, we can obtain the slope. Finally,  $Q_{st}$  was calculated from the slope. For the calculation of heat of CO<sub>2</sub> adsorption on MC and 10MgO/MC, we measured CO<sub>2</sub> adsorption at 283 K and 303 K also (see Fig. 7(b)). A decrease in CO<sub>2</sub> adsorption capacity was observed on both adsorbents with the increase of temperature. Fig. 8(a) shows the heat of CO<sub>2</sub> adsorption with gas adsorption capacity on MC and 10MgO/MC. The heat of CO<sub>2</sub> adsorption was 36.3–36.0 KJ/mole for MC and 36–34.5 KJ/mole for 10MgO/MC. At low coverage of CO<sub>2</sub>, the heat of CO<sub>2</sub> adsorption for 10MgO/MC was higher than MC. It was due to the strong interaction between MgO and CO<sub>2</sub>. The  $Q_{st}$  was decreased to 34.5 KJ/mole with the increase of CO<sub>2</sub> adsorption. For both adsorbents, the heat of CO<sub>2</sub> adsorption was increased after the minimum with an increase of CO<sub>2</sub> adsorption capacity. It was due to the heterogeneity of the adsorbent.

Adsorption stability of an adsorbent can be known by multiple adsorption cycles. Fig. 8(b) shows multiple CO<sub>2</sub> adsorption cycles of 10MgO/MC at 298 K. Before study of each adsorption cycle, the

adsorbent was degasified at 473 K for 2 h under vacuum. 10MgO/MC showed constant CO<sub>2</sub> adsorption capacity up to five cycles. The CO<sub>2</sub> adsorption of 10MgO/PC was compared with some of the reported adsorbents (Table 3). The CO<sub>2</sub> adsorption capacity value was between the adsorption capacity of NiO supported on mesoporous carbon [16], iron oxide doped MCM-41 [15] and Zeolite-13X [32]. Hence, it is one of the adsorbents that has shown good adsorption capacity and selectivity.

## CONCLUSIONS

Mesoporous carbon and MgO incorporated mesoporous carbon samples were used as an adsorbent for the study of CO<sub>2</sub> capture and separation. The presence of MgO on mesoporous was confirmed by all characterization techniques. 10MgO/MC showed high adsorption of CO<sub>2</sub> 1.68 mmol/g at 298 K, 1 bar, which was higher than MC by electrostatic interaction between CO<sub>2</sub> and MgO. High selectivity of CO<sub>2</sub> over N<sub>2</sub> was 40 and heat of CO<sub>2</sub> adsorption was 36 KJ/mole at low coverage of CO<sub>2</sub> on 10MgO/MC. Stable CO<sub>2</sub> adsorption capacity was maintained in each adsorption cycle. Therefore, mesoporous carbon derived from pongamia pinnata fruit hulls can be used as an adsorbent and support to incorporate metal oxides to study CO<sub>2</sub> adsorption and separation.

## ACKNOWLEDGEMENT

HB and RA acknowledge the Science and Engineering Research



Board, Department of Science and Technology, New Delhi, India for the financial support (Grant No. EMEQ-283/2014).

## REFERENCES

1. S. Hosseini, I. Bayesti, E. Marahel, F. Eghbali Babadi, L. Chuah Abdullah and T. S. Y. Choong, *J. Taiwan Inst. Chem. Eng.*, **52**, 109 (2015).
2. D. Aaron and C. Tsouris, *Sep. Purif. Technol.*, **40**, 321 (2005).
3. M. K. Al Mesfer and M. Danish, *J. Environ. Chem. Eng.*, **6**, 4514 (2018).
4. R. Seabra, A. M. Ribeiro, K. Gleichmann, A. F. P. Ferreira and A. E. Rodrigues, *Micropor. Mesopor. Mater.*, **277**, 105 (2019).
5. J. Pires, M. Bestileiro, M. Pinto and A. Gil, *Sep. Purif. Technol.*, **61**, 161 (2008).
6. C. Knöfel, J. Descarpentries, A. Benzaouia, V. Zelenák, S. Mornet, P. L. Llewellyn and V. Hornebecq, *Micropor. Mesopor. Mater.*, **99**, 79 (2007).
7. B. B. Saha, S. Jribi, S. Koyama and I. I. El-Sharkawy, *J. Chem. Eng. Data*, **56**, 1974 (2011).
8. I. I. Gurten, M. Ozmak, E. Yagmur and Z. Aktas, *Biomass Bioenergy*, **37**, 73 (2012).
9. S. Rattanapan, J. Srikram and P. Kongsune, *Energy Procedia*, **138**, 949 (2017).
10. H. Deng, G. Li, H. Yang, J. Tang and J. Tang, *Chem. Eng. J.*, **163**, 373 (2010).
11. T. Uysal, G. Duman, Y. Onal, I. Yasa and J. Yanik, *J. Anal. Appl. Pyrolysis*, **108**, 47 (2014).
12. S. M. Yakout and G. Sharaf El-Deen, *Arabian J. Chem.*, **9**, S1155 (2016).
13. X. Zhao, W. Li, F. Kong, H. Chen, Z. Wang, S. Liu and C. Jin, *Mater. Chem. Phys.*, **219**, 461 (2018).
14. Y. Gao, L. Li, Y. Jin, Y. Wang, C. Yuan, Y. Wei, G. Chen, J. Ge and H. Lu, *Appl. Energy*, **153**, 41 (2015).
15. K. C. Chanapaththarapol, S. Krachumram and S. Youngme, *Micropor. Mesopor. Mater.*, **245**, 8 (2017).
16. M. Li, K. Huang, J. A. Schott, Z. Wu and S. Dai, *Micropor. Mesopor. Mater.*, **249**, 34 (2017).
17. B. J. Kim, K. S. Cho and S. J. Park, *J. Colloid Interface Sci.*, **342**, 575 (2010).
18. D. I. Jang and S. J. Park, *Fuel*, **102**, 439 (2012).
19. J. Shi, N. Yan, H. Cui, Y. Liu and Y. Weng, *J. Environ. Chem. Eng.*, **5**, 4605 (2017).
20. W. Cai, S. Zhang, X. Hu and M. Jaroniec, *Energy Fuels*, **32**, 9701 (2018).
21. H. Zhao, W. Yan, Z. Bian, J. Hu and H. Liu, *Solid State Sci.*, **14**, 250 (2012).
22. H. Jeon, Y. J. Min, S. H. Ahn, S.-M. Hong, J. S. Shin, J. H. Kim and K. B. Lee, *Colloids Surf., A*, **414**, 75 (2012).
23. M. A. Islam, S. Sabar, A. Benhouria, W. A. Khanday, M. Asif and B. H. Hameed, *J. Taiwan Inst. Chem. Eng.*, **74**, 96 (2017).
24. B. Chen, Z. Yang, G. Ma, D. Kong, W. Xiong, J. Wang, Y. Zhu and Y. Xia, *Micropor. Mesopor. Mater.*, **257**, 1 (2018).
25. S. J. Park and S. Y. Lee, *J. Colloid Interface Sci.*, **346**, 194 (2010).
26. S. Brunauer, P. H. Emmett and E. Teller, *J. Am. Chem. Soc.*, **60**, 309 (1938).
27. W. Tian, Q. Gao, Y. Tan, K. Yang, L. Zhu, C. Yang and H. Zhang, *J. Mater. Chem. A*, **3**, 5656 (2015).
28. S. Cheng, L. Zhang, H. Xia and J. Peng, *Green Process. Synth.*, **6**, 487 (2017).
29. M. Saleh, J. N. Tiwari, K. C. Kemp, M. Yousuf and K. S. Kim, *Environ. Sci. Technol.*, **47**, 5467 (2013).
30. C. Goel, H. Bhunia and P. K. Bajpai, *J. Environ. Chem. Eng.*, **4**, 346 (2016).
31. J. Yan, Y. Yu, C. Ma, J. Xiao, Q. Xia, Y. Li and Z. Li, *Appl. Therm. Eng.*, **84**, 118 (2015).
32. J. McEwen, J. D. Hayman and A. Ozgur Yazaydin, *Chem. Phys.*, **412**, 72 (2013).
33. K. Upendar, T. V. Sagar, G. Raveendra, N. Lingaiah, B. V. S. K. Rao, R. B. N. Prasad and P. S. S. Prasad, *RSC Adv.*, **4**, 7142 (2014).
34. S. Zhang, W. Cai, J. Yu, C. Ji and N. Zhao, *Chem. Eng. J.*, **310**, 216 (2017).






## Porous carbon supported calcium oxide for CO<sub>2</sub> adsorption and separation of CO<sub>2</sub>/CH<sub>4</sub>

Madhavi Jonnalagadda , Sobhy M. Ibrahim , Omar H. M. Shair & Suresh Mutyala

To cite this article: Madhavi Jonnalagadda , Sobhy M. Ibrahim , Omar H. M. Shair & Suresh Mutyala (2020): Porous carbon supported calcium oxide for CO<sub>2</sub> adsorption and separation of CO<sub>2</sub>/CH<sub>4</sub> , Environmental Technology, DOI: [10.1080/09593330.2020.1791973](https://doi.org/10.1080/09593330.2020.1791973)

To link to this article: <https://doi.org/10.1080/09593330.2020.1791973>

 View supplementary material 

 Accepted author version posted online: 03 Jul 2020.  
Published online: 16 Jul 2020.

 Submit your article to this journal 

 Article views: 7

 View related articles 

 View Crossmark data 



## Porous carbon supported calcium oxide for CO<sub>2</sub> adsorption and separation of CO<sub>2</sub>/CH<sub>4</sub>

Madhavi Jonnalagadda<sup>a,b</sup>, Sobhy M. Ibrahim<sup>c,d</sup>, Omar H. M. Shair<sup>e</sup> and Suresh Mutyala<sup>f</sup>

<sup>a</sup>Department of Chemistry, Government Degree College for Women, Affiliated to Satavahana University, Karimnagar, India; <sup>b</sup>Department of Chemistry, Sri Ramachandra Arts & Science College, Affiliated to Kakatiya University, Karimnagar, India; <sup>c</sup>Department of Biochemistry, College of Science, King Saud University, Riyadh, Saudi Arabia; <sup>d</sup>Department of Analytical Chemistry and Control, Hot Laboratories and Waste Management Center, Atomic Energy Authority, Cairo, Egypt; <sup>e</sup>Department of Botany and Microbiology, College of Science, King Saud University, Riyadh, Saudi Arabia; <sup>f</sup>Department of Applied and Environmental Chemistry, Interdisciplinary Excellence Centre, University of Szeged, Szeged, Hungary

### ABSTRACT

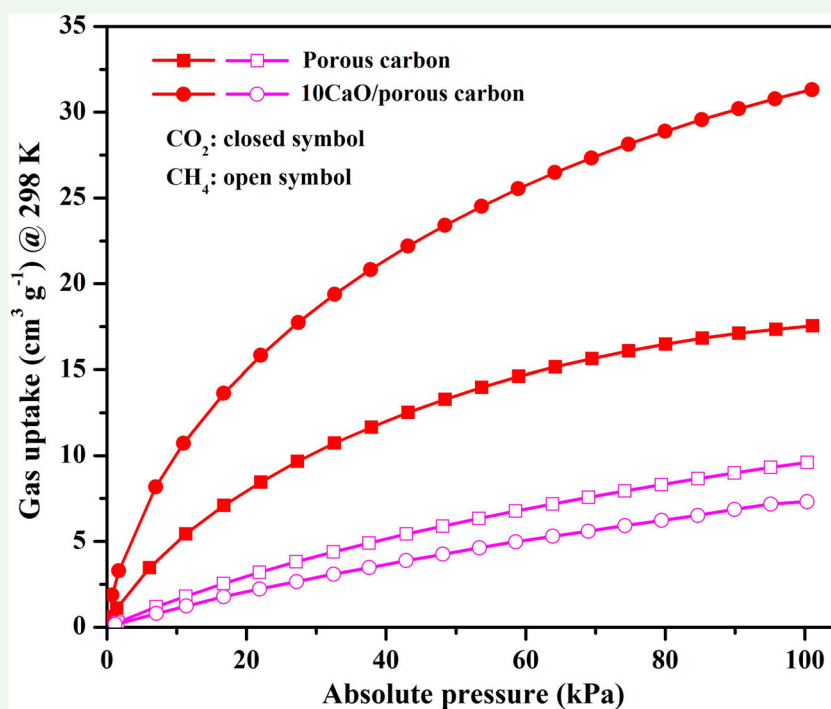
Calcium oxide incorporated porous carbon materials were synthesized by the impregnation method to study CO<sub>2</sub> adsorption and separation of CO<sub>2</sub>/CH<sub>4</sub>. The X-ray diffraction, Raman analysis, N<sub>2</sub> isotherms at 77 K, and SEM with EDX analysis were used to characterize synthesized materials. XRD and N<sub>2</sub> isotherm results have confirmed that synthesized carbon has porosity, and EDX analysis has reported that the presence of CaO on porous carbon. 10CaO/porous carbon has shown 31 cm<sup>3</sup> g<sup>-1</sup> of CO<sub>2</sub> adsorption which was higher than bare porous carbon CO<sub>2</sub> adsorption 17.5 cm<sup>3</sup> g<sup>-1</sup> at 298 K, 1 bar. It was attributed to electrostatic interaction between CaO and CO<sub>2</sub>. However, CH<sub>4</sub> adsorption was decreased by a decrease in surface area. The selectivity of CO<sub>2</sub>/CH<sub>4</sub> was higher for 10CaO/porous carbon and the heat of CO<sub>2</sub> adsorption was 36 KJ/mol at high adsorption of CO<sub>2</sub>. Moreover, CO<sub>2</sub> adsorption was the same in each adsorption cycle.



### ARTICLE HISTORY

Received 29 April 2020  
Accepted 28 June 2020

### KEYWORDS

CaO; porous carbon; carbon dioxide; adsorption and separation; heat of adsorption



**CONTACT** Madhavi Jonnalagadda  madhavi0521@gmail.com  Department of Chemistry, Government Degree College for Women, Affiliated to Satavahana University, Karimnagar 505001, Telangana, India; Department of Chemistry, Sri Ramachandra Arts & Science College, Affiliated to Kakatiya University, Karimnagar 505001, Telangana, India

 Supplemental data for this article can be accessed <https://doi.org/10.1080/09593330.2020.1791973>

© 2020 Informa UK Limited, trading as Taylor & Francis Group

## 1. Introduction

CO<sub>2</sub> is one of the pollutant gases which causes global warming worldwide [1]. It is liberated by the consumption of fossil fuel and the high growth of petrochemical and coal industries. The concentration of CO<sub>2</sub> in the atmosphere can be diminished by absorption, membrane separation, and adsorption techniques [2–4]. Out of these, adsorption is the most prominent method which reduces the high consumption of energy for the regeneration and no corrosion of the equipment. Adsorbents such as activated carbon [5], silica [6], clay [7,8] and zeolites [9–11] were used for CO<sub>2</sub> adsorption and separation. The activated carbon material was hindered because of the unavailability of renewable sources. So, researchers have been using other resources such as rice husk [12], cotton stalk [13], waste tea [14], pongamia pinnata fruit hulls [15] and biodiesel solid residue [16] to synthesize carbon material.

Among these, we have chosen pongamia pinnata fruit hulls to synthesize porous carbon by pyrolysis. The carbon material can be used in research areas such as catalysis [17], gas adsorption and separation [18,19], and optical property study [20]. In the gas adsorption study, the adsorption capacity of carbon material can be increased by the incorporation of metal oxide [21]. Isahak et al have studied CO<sub>2</sub> adsorption using Cu-MgO/carbon nanocomposite and reported 58.5 cm<sup>3</sup> g<sup>-1</sup> of CO<sub>2</sub> adsorption at 303 K, 1 bar [22]. Chamila et al have synthesized mesoporous MgO-SiO<sub>2</sub> composite for CO<sub>2</sub> adsorption at ambient and elevated temperatures. The CO<sub>2</sub> adsorption capacity was 40.3 cm<sup>3</sup> g<sup>-1</sup> at 298 K, 1 bar by physisorption [23]. Kenji et al have also reported CO<sub>2</sub> adsorption capacity 40 cm<sup>3</sup> g<sup>-1</sup> for ZnO supported on activated carbon at 303 K, 1 bar [24].

Recently, our research group has studied CO<sub>2</sub> adsorption and separation of CO<sub>2</sub>/N<sub>2</sub> on MgO incorporated mesoporous carbon and reported 37.6 cm<sup>3</sup> g<sup>-1</sup> of CO<sub>2</sub> adsorption at 298 K, 1 bar [25]. In the above reported all adsorbents, CO<sub>2</sub> adsorption was higher on composite material compared to bulk material due to the electrostatic interaction between adsorbent and CO<sub>2</sub>. In this article, we have studied CaO incorporated porous carbon for CO<sub>2</sub>, CH<sub>4</sub> adsorption, and separation of CO<sub>2</sub>/CH<sub>4</sub>. Along with this, the selectivity of CO<sub>2</sub>/CH<sub>4</sub>, heat of CO<sub>2</sub> adsorption, CO<sub>2</sub> adsorption cycles were also studied.

## 2. Experimental

### 2.1. Chemicals

Chemicals such as calcium nitrate tetrahydrate (Ca(NO<sub>3</sub>)<sub>3</sub>·4H<sub>2</sub>O, ≥99%) and phosphoric acid (H<sub>3</sub>PO<sub>4</sub>, 85 wt%) were purchased from M/s. Sigma-Aldrich,

India, and used without purification. Pongamia pinnata fruit hulls were purchased from a local vendor, India. Double distilled water was used for the synthesis of adsorbents. Gas cylinders such as carbon dioxide, nitrogen, helium, and methane with ultra-high purity were purchased from the local vendor, India.

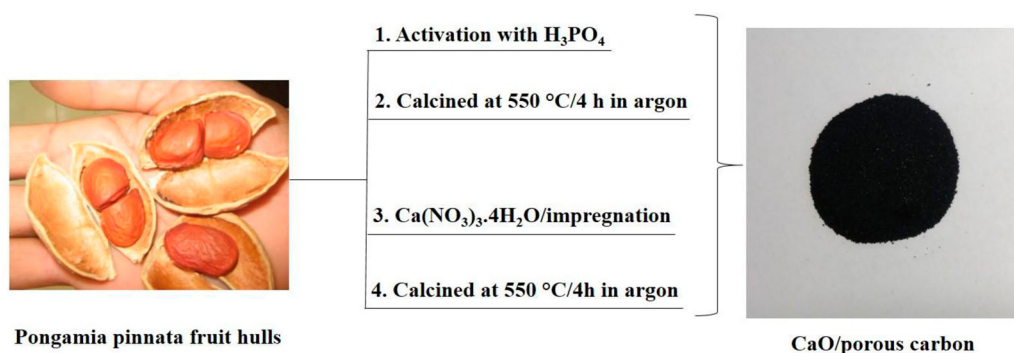
### 2.2. Synthesis of porous carbon and CaO/porous carbon

Porous carbon was synthesized from pongamia pinnata fruit hulls by activation and pyrolysis in inert gas. Firstly, pongamia pinnata fruit hulls were dried and crushed into a fine powder. The powder was activated using phosphoric acid at room temperature for 24 h. The activated sample was calcined at 723 K for 4 h with a heating rate of 10°C/min in argon flow then cooled to room temperature slowly. The obtained sample was washed with distilled water until pH reached to neutral and dried at 373 K for 12 h. Finally, we obtained porous carbon and denoted as PC [26]. Porous carbon supported calcium oxide was synthesized by the impregnation method using calcium nitrate tetrahydrate as a precursor [27]. The desired amount of Ca(NO<sub>3</sub>)<sub>3</sub>·4H<sub>2</sub>O was dissolved in 5 mL distilled water then 1 g of porous carbon was added. The mixture was stirred at room temperature for 1 h then dried at 373 K for 12 h. The dried material was calcined at 723 K for 4 h with a heating rate of 10°C/min in argon flow. Finally, we obtained calcium oxide incorporated porous carbon (Scheme 1). It labelled as xCaO/PC. (x = 2, 5 and 10 wt %).

### 2.3. Characterization

Rigaku Ultima-IV X-ray diffractometer was used to record the X-ray diffractions for each sample using X-ray source having Cu K<sub>α</sub> radiation operated at voltage 40 kV and current 30 mA. The porosity of the sample was determined by measuring N<sub>2</sub> adsorption-desorption isotherms at 77 K using Micromeritics ASAP 2020 Surface area and porosity analyzer. Before isotherm measurement, the sample was activated at 473 K for 2 h under vacuum. Multipoint BET surface area was calculated at P/P<sub>0</sub> = 0.05–0.3 and total pore volume at P/P<sub>0</sub> = 0.99. The t-plot method was used to calculate the micropore volume. Mesopore volume was obtained by subtracting micropore volume from total pore volume. LabRam HR 800 Raman spectrometer was used to record the Raman spectra. Hitachi S-4800 scanning electron microscopy analyzer was used to obtain morphological images and chemical composition of the sample.





**Scheme 1.** Stepwise synthesis of CaO incorporated porous carbon.

## 2.4. Gas adsorption measurement

Micromeritics ASAP 2020 gas adsorption analyzer was used to measure  $CO_2$  and  $CH_4$  adsorption isotherms in low pressure from 0 to 100 kPa at 298 K. Thermostatic bath was connected to water circulating jacket to control sample temperature. Helium gas was used to measure the free space of the sample in the sample tube. About, 0.1 g sample was activated at 473 K for 2 h under vacuum, before measurement of  $CO_2$  and  $CH_4$  adsorption. The initial slope method was used to calculate the selectivity of  $CO_2/CH_4$ . The Clausius–Clapeyron equation was used to calculate the heat of adsorption using adsorption isotherms measured at 283, 298, and 298 K. The  $CO_2$  adsorption cycles were studied by desorbing adsorbed  $CO_2$  in each adsorption cycle at 473 K for 2 h in a vacuum.

## 3. Results and discussion

Figure 1 shows the X-ray diffraction patterns of porous carbon and CaO loaded porous carbon.

Broad diffraction peaks were obtained at  $2\theta = 24.18^\circ$  and  $43.62^\circ$  which were matched with previously reported porous carbon material [28]. In CaO loaded porous carbon material, the major diffraction peaks of porous carbon were present. Along with this, a few new diffraction peaks have appeared with the increase in CaO loading. The diffraction peaks of CaO were  $2\theta = 28.9^\circ$ ,  $32.7^\circ$ ,  $41.3^\circ$ ,  $49.8^\circ$ ,  $54.8^\circ$ , and  $63.1^\circ$  (JCPDS card no. 00-037-1497) [29]. In the low content of CaO, the diffraction peaks of CaO were not undetectable by XRD. Kingkaew et al have reported similar results of iron oxide doped MCM-41 for  $CO_2$  adsorption [30].

The  $N_2$  adsorption–desorption isotherms were measured to know the porosity of the synthesized materials. Figure 2 shows the  $N_2$  adsorption–desorption isotherms of porous carbon and CaO incorporated porous carbon at 77 K. The textural properties such as surface area, pore-volume, and pore size was presented

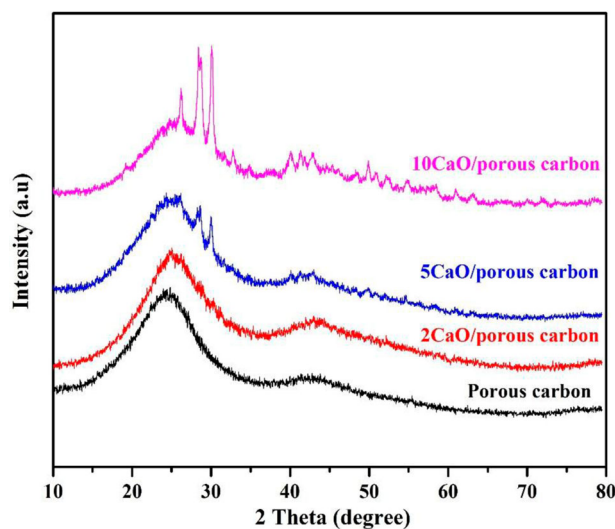


**Figure 1.** XRD patterns of porous carbon and CaO incorporated porous carbon.

in Table 1. The bulk porous carbon material has shown a high amount of  $N_2$  adsorption below the relative pressure 0.1 and a hysteresis loop in between the relative pressure 0.4–1. From the classification of porous materials by IUPAC, the isotherm pattern of bulk porous carbon comes to the category of type-I and type-IV which indicated that the presence of micro and mesopores in the synthesized carbon material [31]. The specific surface area, pore-volume, and pore size of porous carbon were  $630 \text{ m}^2 \text{ g}^{-1}$ ,  $0.72 \text{ cm}^3 \text{ g}^{-1}$  and 4.6 nm respectively. In CaO incorporated porous carbon materials,  $N_2$  adsorption was decreased with an increase in CaO loading. It was attributed to the blockage of pores by incorporated CaO. Consequently, there was a change in the textural properties. The specific surface area was decreased to  $494 \text{ m}^2 \text{ g}^{-1}$ , pore volume to  $0.48 \text{ cm}^3 \text{ g}^{-1}$  and pore size to 3.9 nm.

Raman spectra of porous carbon and 10CaO/porous carbon were shown in Figure 3. Two Raman bands were obtained at  $1337$  and  $1585 \text{ cm}^{-1}$  which correspond

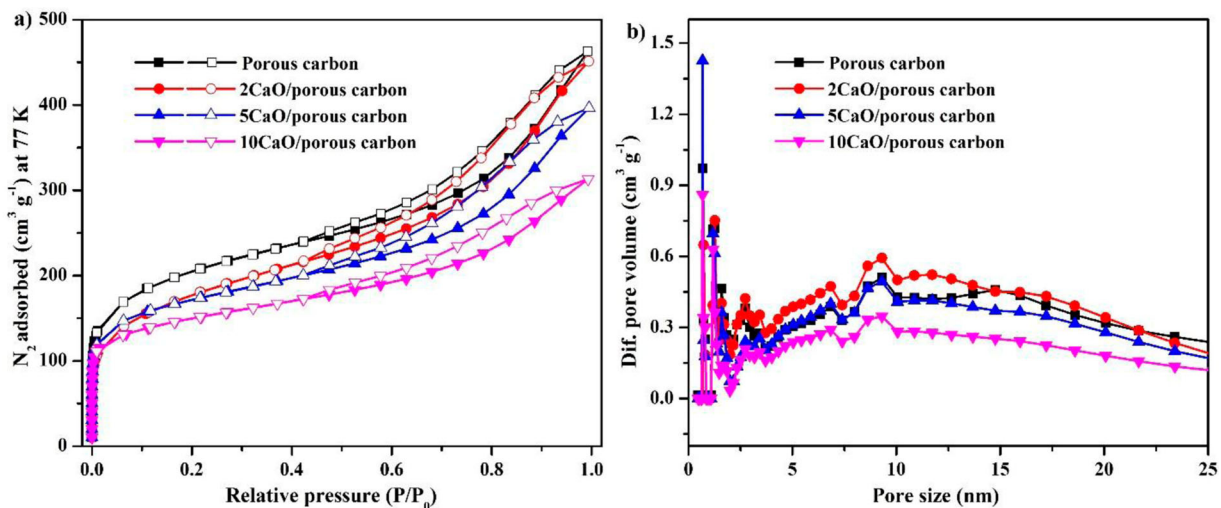


**Figure 2.** (a) N<sub>2</sub> adsorption-desorption isotherms at 77 K (closed symbol: adsorption; open symbol: desorption) and (b) pore size distribution of porous carbon and CaO incorporated porous carbon.

**Table 1.** Textural properties of all synthesized adsorbents.

Sample	$S_{\text{BET}}^{\text{a}}$ (m <sup>2</sup> g <sup>-1</sup> )	$V_{\text{total}}^{\text{b}}$ (cm <sup>3</sup> g <sup>-1</sup> )	$V_{\text{meso}}^{\text{c}}$ (cm <sup>3</sup> g <sup>-1</sup> )	$V_{\text{micro}}^{\text{d}}$ (cm <sup>3</sup> g <sup>-1</sup> )	Pore size <sup>e</sup> (nm)
Porous carbon	630	0.72	0.61	0.11	4.6
2CaO/porous carbon	616	0.70	0.65	0.05	4.5
5CaO/porous carbon	571	0.61	0.49	0.12	4.3
10CaO/porous carbon	494	0.48	0.37	0.11	3.9

<sup>a</sup>BET surface area, <sup>b</sup>Total pore volume at P/P<sub>0</sub> = 0.98, <sup>c</sup>Mesopore volume =  $V_{\text{total}} - V_{\text{micro}}$ , <sup>d</sup>Micropore volume by t-plot method, <sup>e</sup>Average pore size by BET.

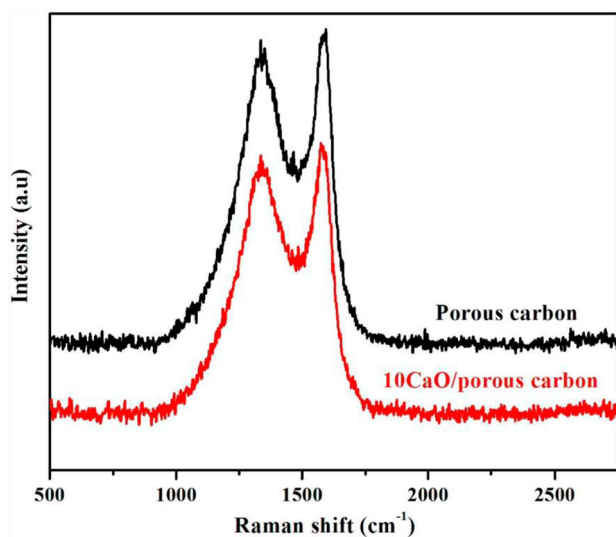


**Figure 3.** Raman spectra of porous carbon and 10CaO/porous carbon.

to D-band and G-band respectively and the intensity of G-band was higher [32]. The ratio of the intensity of D and G-bands for porous carbon and 10CaO/porous carbon was 0.91 and 0.94 respectively. It indicated that a decrease in the graphitic nature of porous carbon material by the incorporation of CaO. Morphological images and chemical composition of porous carbon and 10CaO/porous carbon were measured using SEM with EDX and showed in Figure 4. Disordered carbon particles were observed in porous carbon material (Figure 4a). The incorporated CaO has covered the surface of disordered porous carbon material (Figure 4b). From EDX analysis, the wt% of the calcium in 10CaO incorporated porous carbon material was 0.93 wt%. In both samples, phosphorous was also detected due to the use of phosphoric acid in the activation of dry pongamia pinnata fruit hulls.

The CO<sub>2</sub> adsorption for all synthesized samples was shown in Figure 5a. With the increase of pressure, the amount of CO<sub>2</sub> adsorption capacity was increased and no equilibrium was attained. The CO<sub>2</sub> adsorption for bulk porous carbon was 17.5 cm<sup>3</sup> g<sup>-1</sup> at 298 K, 1 bar. For CaO incorporated porous carbon, the CO<sub>2</sub> adsorption was higher compared with bulk porous carbon. Moreover, the CO<sub>2</sub> adsorption was also increased with an increase of CaO loading. It was due to the electrostatic interaction between CaO and acidic CO<sub>2</sub> molecules. The CO<sub>2</sub> adsorption capacity for CaO incorporated porous carbon samples was 20 cm<sup>3</sup> g<sup>-1</sup> for 2CaO/porous carbon, 23 cm<sup>3</sup> g<sup>-1</sup> for 5CaO/porous carbon, and 31 cm<sup>3</sup> g<sup>-1</sup> for 10CaO/porous carbon at 298 K, 1 bar. High CO<sub>2</sub> adsorption was obtained for 10CaO/

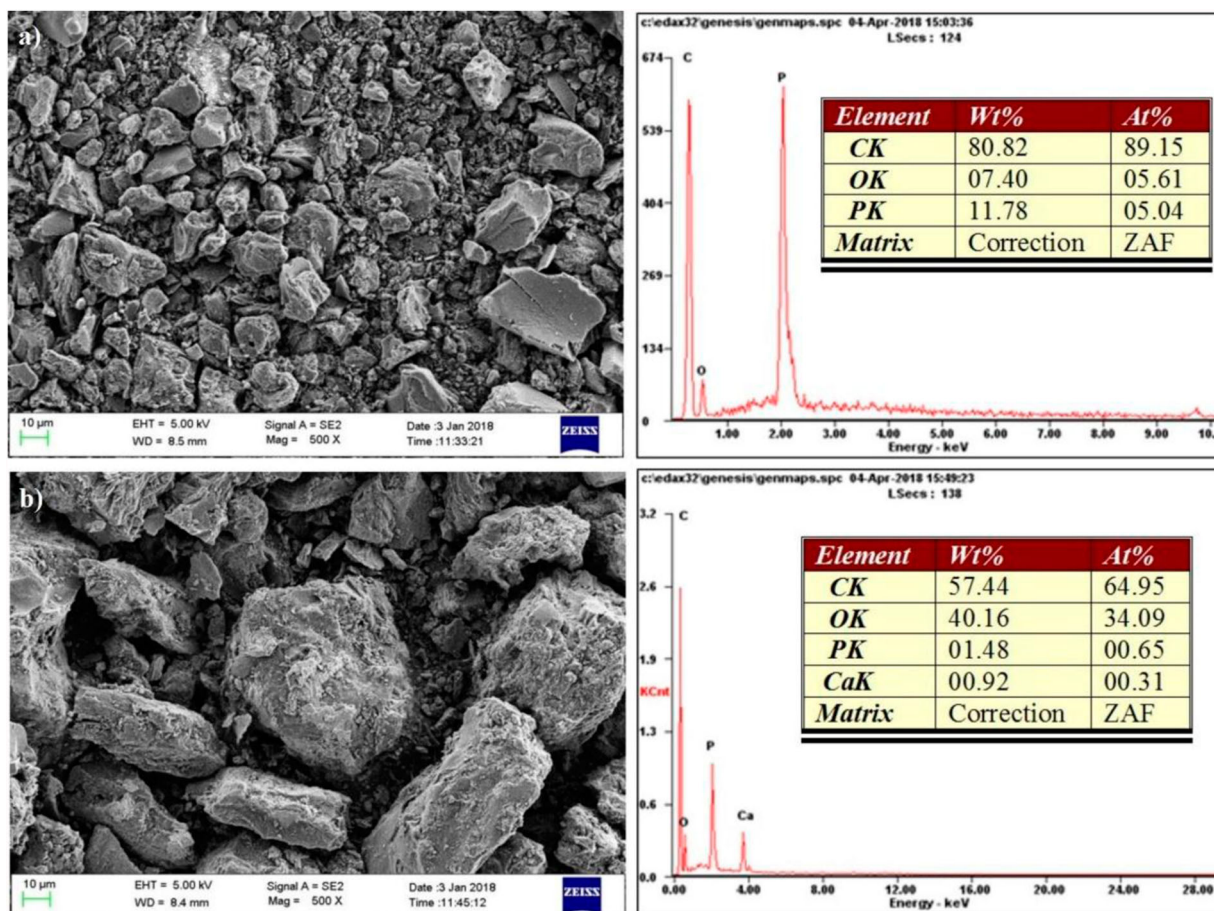


Figure 4. SEM with EDX of (a) porous carbon and (b) 10CaO/porous carbon.

porous carbon by the presence of more number of CaO molecules.

In CaO incorporated porous carbon samples, CO<sub>2</sub> adsorption was dependent on surface chemistry (nature) of the material instead of surface area. We have confirmed by calculation of CO<sub>2</sub> adsorption per unit surface area of the adsorbent (Figure S1). The CO<sub>2</sub> adsorption per unit surface area was higher for CaO incorporated porous carbon compared with bulk porous carbon. Apart from CO<sub>2</sub> adsorption, we have also measured CH<sub>4</sub> adsorption for porous carbon and 10CaO/porous carbon similar to the CO<sub>2</sub> adsorption study (Figure 5b). CH<sub>4</sub> adsorption was increased with an increase in pressure. For porous carbon, CH<sub>4</sub> adsorption was 9.6 and 7 cm<sup>3</sup> g<sup>-1</sup> for 10CaO/porous carbon at 298 K, 1 bar. CH<sub>4</sub> adsorption was decreased in 10CaO/porous carbon by the decrease in surface area and no interaction between adsorbent and CH<sub>4</sub> molecule.

The change in CO<sub>2</sub> and CH<sub>4</sub> adsorption capacity of porous carbon and 10CaO/porous carbon was useful to calculate the selectivity of CO<sub>2</sub>/CH<sub>4</sub>. The initial slope method was used to calculate the selectivity [33,34]. It was shown in Figure 6. The selectivity of CO<sub>2</sub>/CH<sub>4</sub> for

porous carbon and 10CaO/porous carbon was 3 and 9 respectively at 298 K, 1 bar. The CO<sub>2</sub>/CH<sub>4</sub> selectivity obtained on 10CaO/porous carbon was higher than some of the previously reported adsorbents such as ZIF-68 [35], MOF-177 [36], and PAF-1 [37]. The experimental CO<sub>2</sub> adsorption data of porous carbon and 10CaO/porous carbon was fitted with the Langmuir-Freundlich model and the Freundlich model to know the adsorption behaviour of CO<sub>2</sub> (Figure S2) [38]. The fitting model equations were presented in supplementary material and fitting parameter values were presented in Table S1. Good fitting was obtained in the Langmuir-Freundlich model with regression coefficient  $R^2 > 0.999$  and maximum CO<sub>2</sub> adsorption capacity ( $Q_{max}$ ) was higher for 10CaO/porous carbon.

The heat of adsorption is an important parameter in gas adsorption studies. From the heat of adsorption, we can know the interaction of adsorbate with the adsorbent. It can be calculated using the Clausius–Clapeyron equation reported in the reported article [39].

$$\ln P = - \frac{Q_{st}}{RT} + C$$

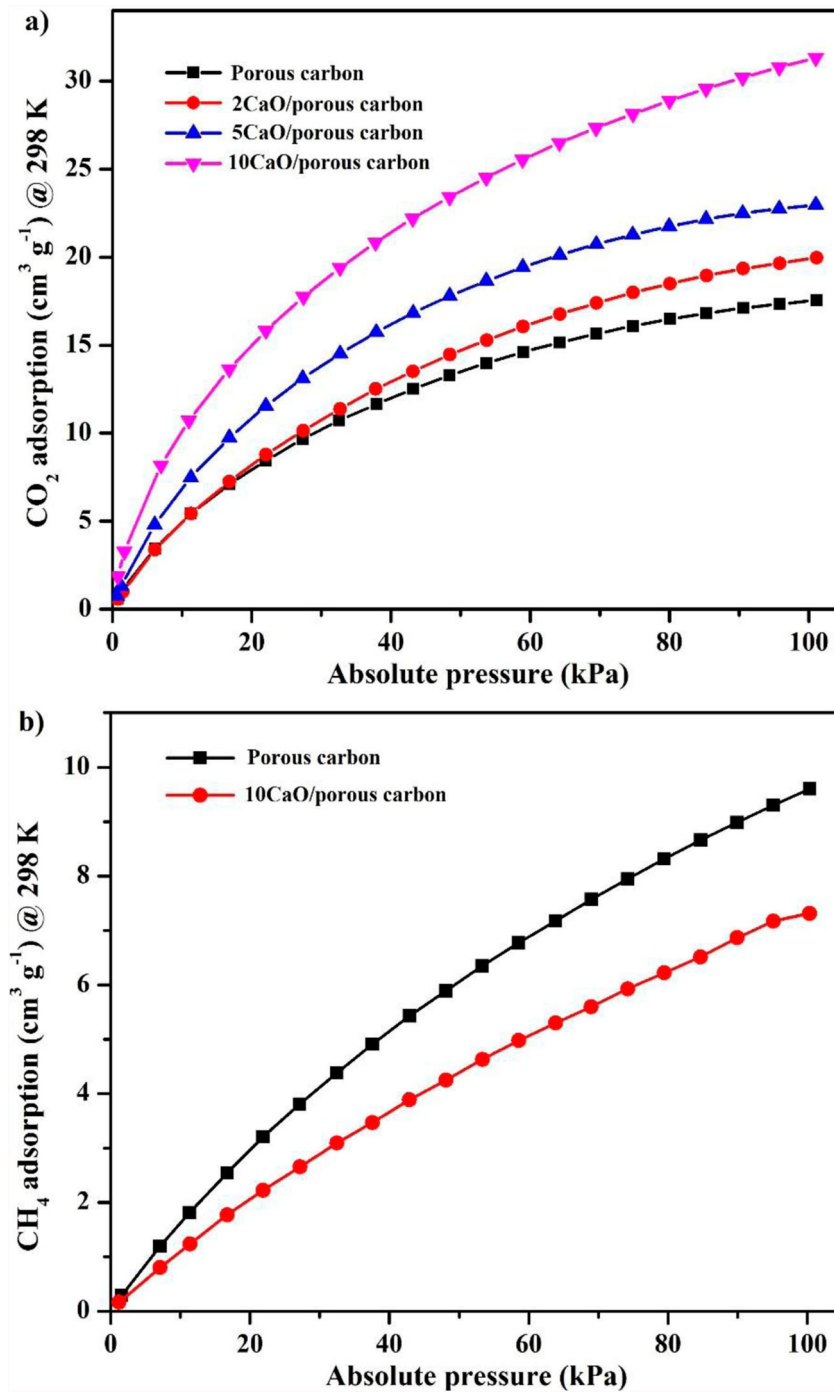


**Figure 5.** (a) CO<sub>2</sub> adsorption of porous carbon and CaO incorporated porous carbon at 298 K (b) CH<sub>4</sub> adsorption of porous carbon and 10CaO/porous carbon at 298 K.

Where  $Q_{st}$  is the heat of adsorption (KJ/mol),  $R$  is the universal gas constant (8.314 J/K.mol),  $P$  is pressure (kPa),  $T$  is the temperature (K) and  $C$  is constant. The slope obtained by drawing a graph between  $\ln P$  vs  $1/T$  with straight line fitting was used to calculate the heat of adsorption. To calculate the heat of CO<sub>2</sub> adsorption for 10CaO/porous carbon, CO<sub>2</sub> adsorption at 283 and 303 K was also measured (Figure S3). With an increase in temperature, CO<sub>2</sub> adsorption was decreased by an increase in the

kinetic energy of CO<sub>2</sub>. The heat of CO<sub>2</sub> adsorption for 10CaO/porous carbon was shown in Figure 7a. The  $Q_{st}$  was 20–36 KJ/mol. At high adsorption of CO<sub>2</sub>,  $Q_{st}$  was higher due to the non-uniform distribution of CaO on the surface of porous carbon material.

The CO<sub>2</sub> adsorption cycles of 10CaO/porous carbon were shown in Figure 7b to know the CO<sub>2</sub> adsorption stability. Before the study of each adsorption cycle, the sample was heated at 473 K for 2 h under vacuum



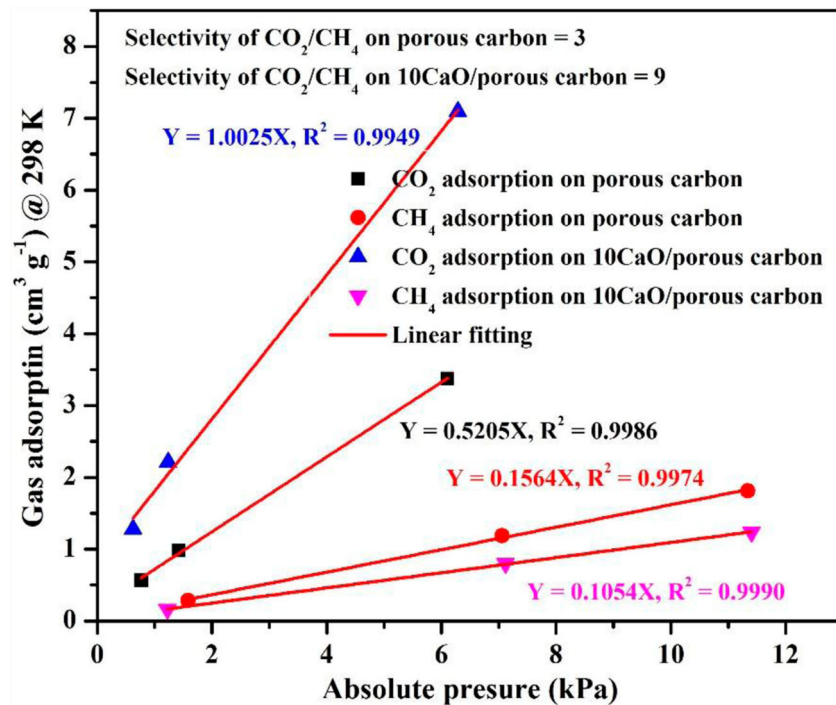


Figure 6. CO<sub>2</sub>/CH<sub>4</sub> selectivity of porous carbon and 10CaO/porous carbon.

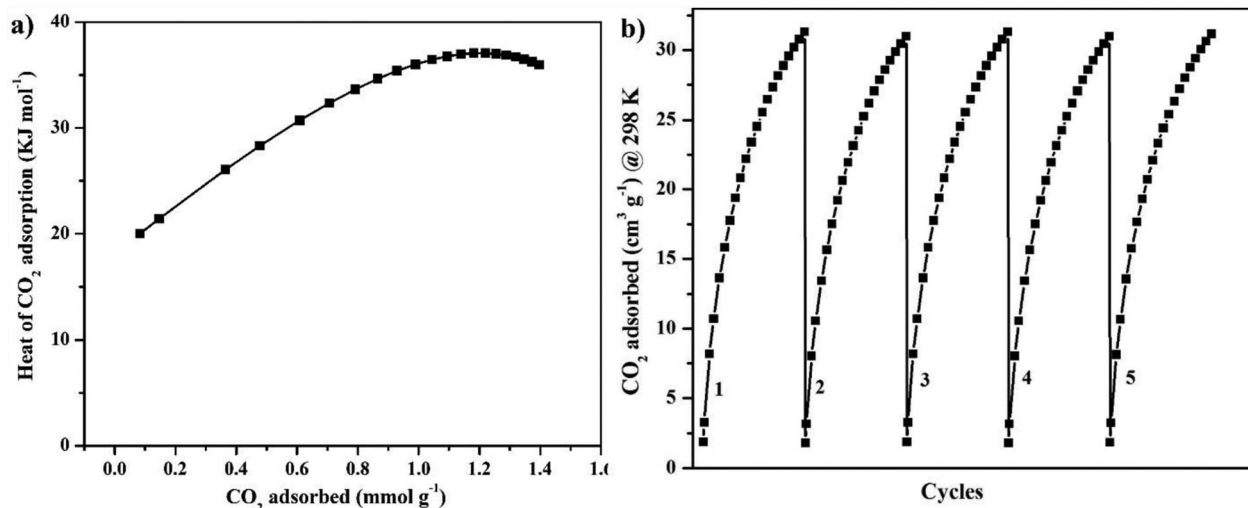


Figure 7. (a) The heat of CO<sub>2</sub> adsorption and (b) CO<sub>2</sub> adsorption cycles of 10CaO/porous carbon.

Table 2. Comparison of CO<sub>2</sub> adsorption of 10CaO/porous carbon in reported articles.

Adsorbent	Adsorption method	CO <sub>2</sub> adsorbed at 298 K, 1 bar (cm <sup>3</sup> g <sup>-1</sup> )	Reference
Zeolite-13X	Volumetric	38	[42]
CuO/polymer	Volumetric	28	[43]
Amine modified Mg-Al LDH	Gravimetric	26	[44]
Mesoporous Al <sub>2</sub> O <sub>3</sub> -organosilica	Volumetric	22	[40]
Mesoporous CaO-SiO <sub>2</sub>	Volumetric	38	[23]
CaO/porous carbon	Volumetric	31	Present work

to remove adsorbed CO<sub>2</sub>. The CO<sub>2</sub> adsorption capacity was constant in each adsorption cycle which indicated that the adsorbent has good adsorption stability. 10CaO/porous carbon CO<sub>2</sub> adsorption capacity was compared with previously reported adsorbents CO<sub>2</sub> adsorption capacity (Table 2). It was in between CO<sub>2</sub> adsorption capacity of mesoporous Al<sub>2</sub>O<sub>3</sub>-organosilica [40], mesoporous CaO-SiO<sub>2</sub> [41], and mesoporous MgO-Al<sub>2</sub>O<sub>3</sub> [23]. Hence, CaO incorporated porous carbon is also one of the adsorbents to study CO<sub>2</sub> adsorption and separation.

## 4. Conclusion

In this work, we have synthesized porous carbon and CaO incorporated porous carbon materials to study CO<sub>2</sub> adsorption and separation of CO<sub>2</sub>/CH<sub>4</sub>. High adsorption of CO<sub>2</sub> was obtained for CaO incorporated porous carbon compared with bulk porous carbon because of electrostatic interaction between CaO and CO<sub>2</sub>. Moreover, the selectivity of CO<sub>2</sub>/CH<sub>4</sub> was also higher for 10CaO incorporated porous carbon. The heat of CO<sub>2</sub> adsorption was 36 KJ/mole at high coverage of CO<sub>2</sub> by non-uniform distribution of CaO on the porous carbon support. The CO<sub>2</sub> adsorption capacity was constant for 10CaO/porous carbon in multiple adsorption cycles. Therefore, porous carbon supported basic metal oxides can be used for CO<sub>2</sub> adsorption and separation.

## Acknowledgment

MJ acknowledges the SERB, Department of Science and Technology, New Delhi, India for financial support (EMEQ-283/2014). This work was supported by Researchers supporting project number (RSP-2019/100), King Saud University, Riyadh, Saudi Arabia.

## Disclosure statement

No potential conflict of interest was reported by the author(s).

## Funding

This work was supported by Researchers supporting project number (RSP-2019/100), King Saud University, Riyadh, Saudi Arabia. Science and Engineering Research Board.

## References

- [1] Shukla JB, Verma M, Misra AK. Effect of global warming on sea level rise: a modeling study. *Ecol Complex*. 2017;32:99–110.
- [2] Yuan Y, Rochelle GT. CO<sub>2</sub> absorption rate and capacity of semi-aqueous piperazine for CO<sub>2</sub> capture. *Int J Greenhouse Gas Control*. 2019;85:182–186.
- [3] Li S, Jiang X, Sun H, et al. Mesoporous dendritic fibrous nanosilica (DFNS) stimulating mix matrix membranes towards superior CO<sub>2</sub> capture. *J Memb Sci*. 2019;586:185–191.
- [4] Grande CA, Roussanaly S, Anantharaman R, et al. CO<sub>2</sub> Capture in natural gas production by adsorption processes. *Energy Procedia*. 2017;114:2259–2264.
- [5] Ogungbenro AE, Quang DV, Al-Ali K, et al. Activated carbon from date seeds for CO<sub>2</sub> capture applications. *Energy Procedia*. 2017;114:2313–2321.
- [6] Wang HC, Lu C, Bai H, et al. Pilot-scale production of mesoporous silica-based adsorbent for CO<sub>2</sub> capture. *Appl Surf Sci*. 2012;258:6943–6951.
- [7] Gómez-Pozuelo G, Sanz E, Arencibia A, et al. CO<sub>2</sub> adsorption on amine-functionalized clays. *Microporous Mesoporous Mater*. 2019;282:38–47.
- [8] Yeste MP, Gatica JM, Ahrouch M, et al. Clay honeycomb monoliths as low cost CO<sub>2</sub> adsorbents. *J Taiwan Inst Chem Eng*. 2017;80:415–423.
- [9] Pham T-H, Lee B-K, Kim J, et al. Enhancement of CO<sub>2</sub> capture by using synthesized nano-zeolite. *J Taiwan Inst Chem Eng*. 2016;64:220–226.
- [10] Chen SJ, Zhu M, Fu Y, et al. Using 13X, LiX, and LiPdAgX zeolites for CO<sub>2</sub> capture from post-combustion flue gas. *Appl Energy*. 2017;191:87–98.
- [11] Modak A, Jana S. Advancement in porous adsorbents for post-combustion CO<sub>2</sub> capture. *Microporous Mesoporous Mater*. 2019;276:107–132.
- [12] Cai R, You B, Chen M, et al. Metal-free core-shell structured N-doped carbon/carbon heterojunction for efficient CO<sub>2</sub> capture. *Carbon N Y*. 2019;150:43–51.
- [13] Fang K, Chen M, Chen J, et al. Cotton stalk-derived carbon fiber@Ni-Al layered double hydroxide nanosheets with improved performances for supercapacitors. *Appl Surf Sci*. 2019;475:372–379.
- [14] Wong S, Lee Y, Ngadi N, et al. Synthesis of activated carbon from spent tea leaves for aspirin removal. *Chin J Chem Eng*. 2018;26:1003–1011.
- [15] Tan YL, Abdullah AZ, Hameed BH. Product distribution of the thermal and catalytic fast pyrolysis of karanja (*Pongamia pinnata*) fruit hulls over a reusable silica-alumina catalyst. *Fuel*. 2019;245:89–95.
- [16] Zhao X, Li W, Kong F, et al. Carbon spheres derived from biomass residue via ultrasonic spray pyrolysis for supercapacitors. *Mater Chem Phys*. 2018;219:461–467.
- [17] Fidalgo B, Menéndez JÁ. Carbon materials as catalysts for decomposition and CO<sub>2</sub> reforming of methane: a review. *Chin J Catal*. 2011;32:207–216.
- [18] Du J, Li W-C, Ren Z-X, et al. Synthesis of mechanically robust porous carbon monoliths for CO<sub>2</sub> adsorption and separation. *J Energy Chem*. 2020;42:56–61.
- [19] Modak A, Bhaumik A. Porous carbon derived via KOH activation of a hypercrosslinked porous organic polymer for efficient CO<sub>2</sub>, CH<sub>4</sub>, H<sub>2</sub> adsorptions and high CO<sub>2</sub>/N<sub>2</sub> selectivity. *J Solid State Chem*. 2015;232:157–162.
- [20] Leal NNS, Brandão-Silva AC, Fantini C, et al. Thermo-optical response of colloidal metallic and semiconducting single-walled carbon nanotubes. *Opt Laser Technol*. 2019;116:315–321.
- [21] Li M, Huang K, Schott JA, et al. Effect of metal oxides modification on CO<sub>2</sub> adsorption performance over mesoporous carbon. *Microporous Mesoporous Mater*. 2017;249:34–41.
- [22] Isahak WNRW, Hasan SZ, Ramli ZAC, et al. Enhanced physical and chemical adsorption of carbon dioxide using bimetallic copper–magnesium oxide/carbon nanocomposite. *Res Chem Intermed*. 2018;44:829–841.
- [23] Wang F, Gunathilake C, Jaroniec M. Development of mesoporous magnesium oxide–alumina composites for CO<sub>2</sub> capture. *J CO<sub>2</sub> Util*. 2016;13:114–118.
- [24] Taira K, Nakao K, Suzuki K. CO<sub>2</sub> capture in humid gas using ZnO/activated carbon and ZnO reactivity with CO<sub>2</sub>. *React Kinet, Mech Catal*. 2015;115:563–579.
- [25] Burri H, Anjum R, Gurram RB, et al. Mesoporous carbon supported MgO for CO<sub>2</sub> capture and separation of CO<sub>2</sub>/N<sub>2</sub>. *Korean J Chem Eng*. 2019;36:1482–1488.
- [26] Islam MA, Sabar S, Benhouria A, et al. Nanoporous activated carbon prepared from karanj (*Pongamia pinnata*)

- fruit hulls for methylene blue adsorption. *J Taiwan Inst Chem Eng.* **2017**;74:96–104.
- [27] van Dillen AJ, Terörde RJAM, Lensveld DJ, et al. Synthesis of supported catalysts by impregnation and drying using aqueous chelated metal complexes. *J Catal.* **2003**;216:257–264.
- [28] Liu C, Shi G, Wang G, et al. Preparation and electrochemical studies of electrospun phosphorus doped porous carbon nanofibers. *RSC Adv.* **2019**;9:6898–6906.
- [29] Selva Kumar V, Hua Lee Z, Huey Sim J, et al. Improved CO<sub>2</sub> sorption performance of calcium oxide (CaO) sorbent with nickel oxide additive. *IOP Conf Ser Earth Environ Sci.* **2019**;268:012026.
- [30] Chanapatttharapol KC, Krachuamram S, Youngme S. Study of CO<sub>2</sub> adsorption on iron oxide doped MCM-41. *Microporous Mesoporous Mater.* **2017**;245:8–15.
- [31] Brunauer S, Emmett PH, Teller E. Adsorption of gases in multimolecular layers. *J Am Chem Soc.* **1938**;60:309–319.
- [32] Sogut EG, Acidereli H, Kuyuldar E, et al. Single-walled carbon nanotube supported Pt-Ru bimetallic superb nanocatalyst for the hydrogen generation from the methanolysis of methylamine-borane at mild conditions. *Sci Rep.* **2019**;9:15724.
- [33] Khutia A, Janiak C. Programming MIL-101Cr for selective and enhanced CO<sub>2</sub> adsorption at low pressure by postsynthetic amine functionalization. *Dalton Trans.* **2014**;43:1338–1347.
- [34] Liu Z, Zhu Y, Du Z, et al. Detailed investigation of N-doped microporous carbons derived from urea furfural resin for CO<sub>2</sub> capture. *J Porous Mater.* **2015**;22:1663–1672.
- [35] Phan A, Doonan CJ, Uribe-Romo FJ, et al. Synthesis, structure, and carbon dioxide capture properties of zeolitic imidazolate frameworks. *Acc Chem Res.* **2010**;43:58–67.
- [36] Saha D, Bao Z, Jia F, et al. Adsorption of CO<sub>2</sub>, CH<sub>4</sub>, N<sub>2</sub>O, and N<sub>2</sub> on MOF-5, MOF-177, and Zeolite 5A. *Environ Sci Technol.* **2010**;44:1820–1826.
- [37] Zhang W, Cheng Y, Guo C, et al. Cobalt incorporated porous aromatic framework for CO<sub>2</sub>/CH<sub>4</sub> separation. *Ind Eng Chem Res.* **2018**;57:10985–10991.
- [38] Mutyala S, Yakout SM, Ibrahim SS, et al. Enhancement of CO<sub>2</sub> capture and separation of CO<sub>2</sub>/N<sub>2</sub> using post-synthetic modified MIL-100(Fe). *New J Chem.* **2019**;43:9725–9731.
- [39] Xu F, Yu Y, Yan J, et al. Ultrafast room temperature synthesis of GrO@HKUST-1 composites with high CO<sub>2</sub> adsorption capacity and CO<sub>2</sub>/N<sub>2</sub> adsorption selectivity. *Chem Eng J.* **2016**;303:231–237.
- [40] Gunathilake C, Jaroniec M. Mesoporous alumina–zirconia–organosilica composites for CO<sub>2</sub> capture at ambient and elevated temperatures. *J Mater Chem A.* **2015**;3:2707–2716.
- [41] Gunathilake C, Jaroniec M. Mesoporous calcium oxide–silica and magnesium oxide–silica composites for CO<sub>2</sub> capture at ambient and elevated temperatures. *J Mater Chem A.* **2016**;4:10914–10924.
- [42] McEwen J, Hayman J-D, Ozgur Yazaydin A. A comparative study of CO<sub>2</sub>, CH<sub>4</sub> and N<sub>2</sub> adsorption in ZIF-8, Zeolite-13X and BPL activated carbon. *Chem Phys.* **2013**;412:72–76.
- [43] Bouhadjar L, Boukoussa B, Kherroub DE, et al. Adsorption behavior of carbon dioxide on new nanocomposite CuO/PPB: effect of CuO content. *J Inorg Organomet Polym Mater.* **2019**;29:326–331.
- [44] Wang J, Stevens LA, Drage TC, et al. Preparation and CO<sub>2</sub> adsorption of amine modified Mg–Al LDH via exfoliation route. *Chem Eng Sci.* **2012**;68:424–431.

# Study of CO<sub>2</sub> adsorption and separation using modified porous carbon

Madhavi Jonnalagadda<sup>1,2,\*</sup> , Rumana Anjum<sup>1</sup>, Harshitha Burri<sup>1</sup> and Suresh Mutyala<sup>3,4,\*</sup>

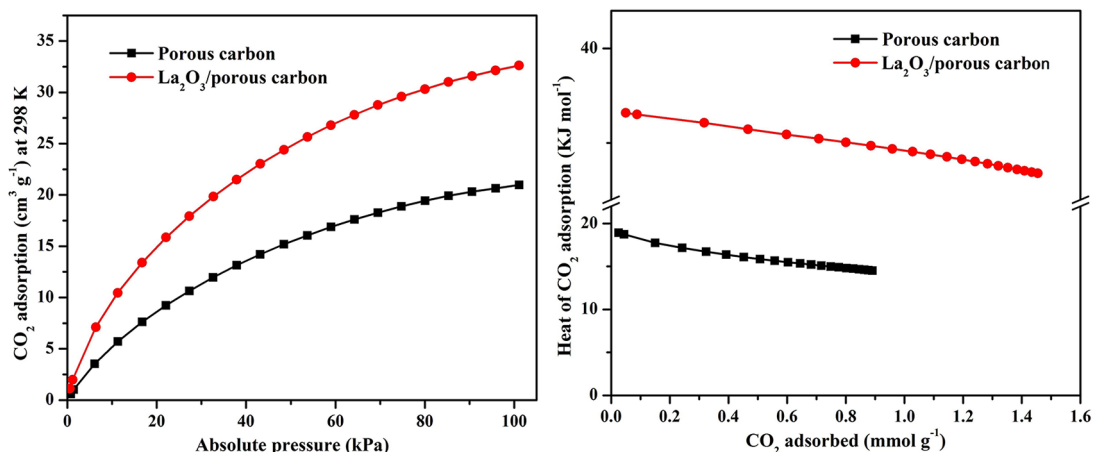
## Abstract

Porous carbon and La<sub>2</sub>O<sub>3</sub>/porous carbon materials are synthesized for the study of CO<sub>2</sub> adsorption and separation by the volumetric method. The synthesized adsorbents are characterized by X-ray diffraction, N<sub>2</sub> adsorption–desorption isotherms, Raman spectra and scanning electron microscopy with energy-dispersive X-ray analysis. Characterization results confirm the existence of porosity in the synthesized carbon materials and uniform distribution of lanthanum(III) oxide on porous carbon. The CO<sub>2</sub> adsorption capacity for porous carbon and La<sub>2</sub>O<sub>3</sub>/porous carbon is 21 and 33 cm<sup>3</sup> g<sup>-1</sup>, respectively, at 298 K and 1 bar. High adsorption of CO<sub>2</sub> is obtained for La<sub>2</sub>O<sub>3</sub>/porous carbon because of the electrostatic interaction between La<sub>2</sub>O<sub>3</sub> and CO<sub>2</sub>. Moreover, the N<sub>2</sub> adsorption capacity is 2.8 cm<sup>3</sup> g<sup>-1</sup> for porous carbon and 2.2 cm<sup>3</sup> g<sup>-1</sup> for La<sub>2</sub>O<sub>3</sub>/porous carbon at 298 K and 1 bar. The change in N<sub>2</sub> adsorption is due to the decrease in surface area. For La<sub>2</sub>O<sub>3</sub>/porous carbon, the selectivity of CO<sub>2</sub>/N<sub>2</sub> is 33.5 and the heat of CO<sub>2</sub> adsorption is 36.5 kJ mol<sup>-1</sup> at low adsorption of CO<sub>2</sub>. It also shows constant CO<sub>2</sub> adsorption capacity in each adsorption cycle.

## Keywords

adsorption cycles, CO<sub>2</sub> capture, heat of adsorption, lanthanum(III) oxide, porous carbon, separation

Date received: 18 April 2020; accepted: 8 June 2020



<sup>1</sup>Department of Chemistry, Government Degree College for Women, Karimnagar, India

<sup>2</sup>Department of Chemistry, Sri Ramachandra Arts & Science College, Kothagudem, India

<sup>3</sup>Department of Applied and Environmental Chemistry, Interdisciplinary Excellence Centre, University of Szeged, Szeged, Hungary

<sup>4</sup>Department of Chemistry and Key Laboratory for Preparation and Application of Ordered Structural Materials of Guangdong Province, Shantou University, Shantou, P.R. China

\*Both authors contributed equally to this work.

## Corresponding authors:

Madhavi Jonnalagadda, Department of Chemistry, Government Degree College for Women, Karimnagar 505001, Telangana, India.  
Email: madhavi0521@gmail.com

Suresh Mutyala, Department of Applied and Environmental Chemistry, Interdisciplinary Excellence Centre, University of Szeged, Rerrich Béla tér 1, 6720 Szeged, Hungary.  
Email: sureshm186@gmail.com



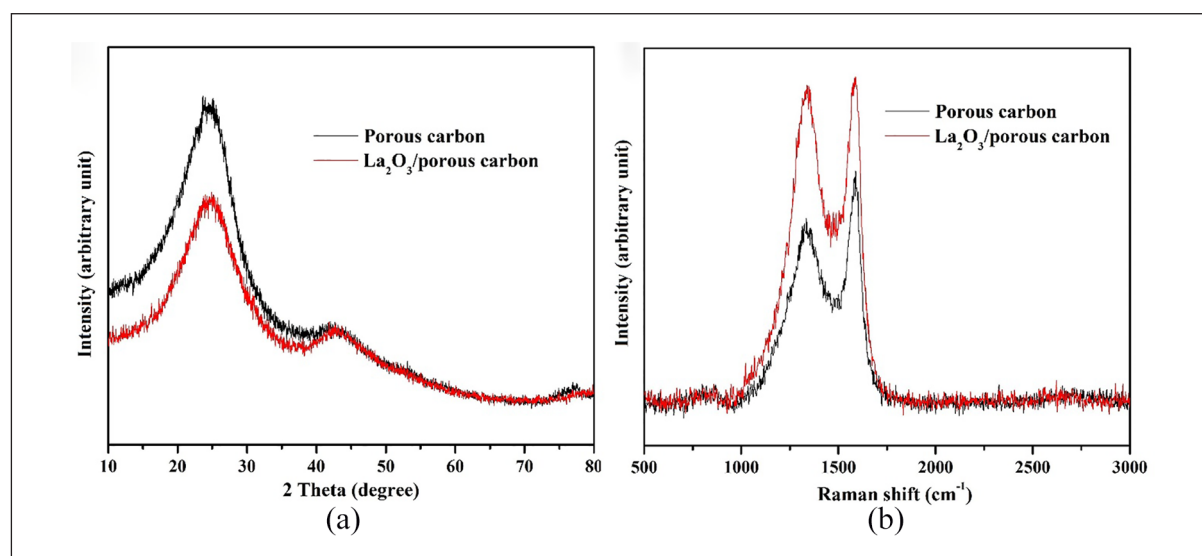


**Figure 1.** (a) XRD patterns, and (b) Raman spectra of porous carbon and  $\text{La}_2\text{O}_3$ /porous carbon.

## Introduction

Global warming is a worldwide environmental issue which is contributed to carbon dioxide. It is liberated by the combustion of fossil fuels coinciding with the high growth of the automobile and petrochemical industries.<sup>1</sup> Day by day, the concentration of  $\text{CO}_2$  is increasing and has reached 400 ppm, which is more than pre-industrial levels. Hence, greater effort has to be made to control the  $\text{CO}_2$  concentration levels in the atmosphere. Carbon capture and separation (CCS) techniques on solid materials is an important method to lower  $\text{CO}_2$  concentration levels, as is the liquid amine solution absorption technique. In power plants, liquid amine solutions are mostly used to capture  $\text{CO}_2$ . However, high energy is required for regeneration and occurs corrosion of the pipeline system. To overcome these drawbacks, solid materials are used for CCS. So far, materials such as activated carbon,<sup>2</sup> zeolites<sup>3</sup> and mesoporous silica<sup>4</sup> have been used for  $\text{CO}_2$  capture and separation.

Activated carbon is a cost-effective adsorbent and has a high surface area. However, the production of activated carbon on a large scale is hindered because of less renewable sources. Porous carbon synthesis from renewable sources is an important aspect. Renewable sources such as sawdust,<sup>5</sup> rice husk,<sup>6</sup> waste tea,<sup>7</sup> biodiesel industry solid residues,<sup>8</sup> cotton stalks,<sup>9</sup> olive and peach stones,<sup>10,11</sup> palm oil ash<sup>12</sup> and coffee grounds<sup>13</sup> have been used to synthesize porous carbon materials. *Pongamia pinnata* fruit seeds are used for the production of biodiesel. During the production of biodiesel, a large quantity of *pongamia pinnata* fruit hulls is disposed of without commercial use. From these, porous carbon can also be synthesized by pyrolysis.

The  $\text{CO}_2$  adsorption of porous carbon can be enhanced by the incorporation of basic metal oxide and a heteroatom, which generates basic sites on the porous carbon. The Nitrogen-doped porous carbon-derived from Hazelnut-shell has shown  $\text{CO}_2$  adsorption capacity of  $97 \text{ cm}^3 \text{ g}^{-1}$  at 298 K and 1 bar.<sup>14</sup> Similarly, D-glucose used as a source for N-doped porous carbon synthesis and

reported  $\text{CO}_2$  adsorption capacity of  $88 \text{ cm}^3 \text{ g}^{-1}$  at 298 K and 1 bar, respectively.<sup>15</sup> Porous carbon derived from sustainable biomass stalk showed  $\text{CO}_2$  adsorption capacity of  $82.5 \text{ cm}^3 \text{ g}^{-1}$  at 298 K and 1 bar.<sup>16</sup> MgO-incorporated mesoporous carbon has shown a  $\text{CO}_2$  adsorption capacity of  $46.8 \text{ cm}^3 \text{ g}^{-1}$  at 298 K and 1 bar<sup>17</sup> and  $\text{CeO}_2$ -doped mesoporous carbon demonstrated  $39.7 \text{ cm}^3 \text{ g}^{-1}$  of  $\text{CO}_2$  adsorption at 303 K and 1 bar.<sup>18</sup> The  $\text{CO}_2$  adsorption was higher on  $\text{Cu}_2\text{O}$  and NiO-incorporated porous carbon compared to bare porous carbon.<sup>19,20</sup> Recently, our group reported mesoporous carbon supported MgO for  $\text{CO}_2$  capture. This material showed  $37.6 \text{ cm}^3 \text{ g}^{-1}$  of  $\text{CO}_2$  adsorption on 10 wt% MgO-incorporated mesoporous carbon which was higher than bare mesoporous carbon  $\text{CO}_2$  adsorption  $20.2 \text{ cm}^3 \text{ g}^{-1}$  at 298 K and 1 bar.<sup>21</sup> For the reported adsorbents, high  $\text{CO}_2$  adsorption was obtained for metal oxide incorporated porous carbon due to the electrostatic interaction between the metal oxide and  $\text{CO}_2$ . In this paper, we have studied the influence of a low content of lanthanum(III) oxide on a porous carbon towards  $\text{CO}_2$  adsorption and separation. Moreover,  $\text{CO}_2/\text{N}_2$  selectivity, heat of  $\text{CO}_2$  adsorption and  $\text{CO}_2$  adsorption cycles were studied.

## Results and discussion

### Structural characterization

Figure 1(a) shows the X-ray diffraction (XRD) of porous carbon and lanthanum oxide incorporated porous carbon. Two broad diffraction peaks were observed at  $2\theta = 24^\circ$  and  $43.5^\circ$  for the (002) and (100) planes, respectively. These were the main characteristic peaks of porous carbon.<sup>22</sup> Moreover, lanthanum oxide-incorporated porous carbon showed diffraction peaks similar to porous carbon and no peaks related to  $\text{La}_2\text{O}_3$  appeared. This indicated that  $\text{La}_2\text{O}_3$  was highly dispersed on porous carbon and/or not detectable by XRD analysis. Chanapaththarapol et al.<sup>23</sup> have also reported similar results with iron oxide doped MCM-41 for  $\text{CO}_2$  adsorption. The Raman spectra of porous carbon and

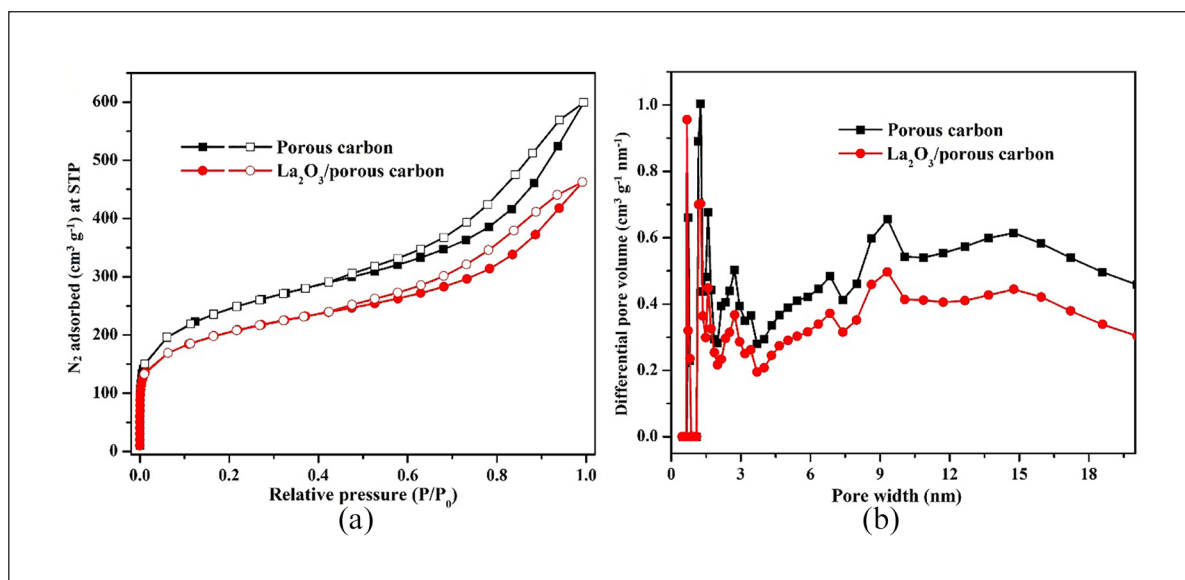


**Figure 2.** (a) N<sub>2</sub> adsorption–desorption isotherms (closed symbol: adsorption, open symbol: desorption) and (b) pore size distribution of porous carbon and La<sub>2</sub>O<sub>3</sub>/porous carbon.

**Table 1.** Textural properties and metal composition of the synthesized samples.

Sample	S <sub>BET</sub> (m <sup>2</sup> g <sup>-1</sup> ) <sup>a</sup>	V <sub>total</sub> (cm <sup>3</sup> g <sup>-1</sup> ) <sup>b</sup>	V <sub>micro</sub> (cm <sup>3</sup> g <sup>-1</sup> ) <sup>c</sup>	V <sub>meso</sub> (cm <sup>3</sup> g <sup>-1</sup> ) <sup>d</sup>	Pore size (nm) <sup>e</sup>	La content (wt%) <sup>f</sup>
Porous carbon	826	0.89	0.12	0.77	4.3	NF
La <sub>2</sub> O <sub>3</sub> /porous carbon	715	0.76	0.10	0.66	4.2	2.97

<sup>a</sup>BET surface area.

<sup>b</sup>Total pore volume at P/P<sub>0</sub> = 0.99.

<sup>c</sup>Micropore volume obtained from the t-plot.

<sup>d</sup>Mesopore volume obtained by subtracting V<sub>micro</sub> from V<sub>total</sub>.

<sup>e</sup>Average pore size by BET.

<sup>f</sup>From EDX, NF: not found.

La<sub>2</sub>O<sub>3</sub>/porous carbon are shown in Figure 1(b). Porous carbon shows Raman bands at 1334 and 1582 cm<sup>-1</sup>, which are related to the D-band and the G-band, respectively.<sup>24</sup> The D-band corresponds to disordered carbon, whereas the G-band corresponds to graphitic carbon. The ratio of the intensity of D and G-bands (I<sub>D</sub>/I<sub>G</sub>) was 0.87 for porous carbon and 0.95 for La<sub>2</sub>O<sub>3</sub>/porous carbon. The high I<sub>D</sub>/I<sub>G</sub> ratio of La<sub>2</sub>O<sub>3</sub>/porous carbon indicates a decrease in the graphitic nature of porous carbon by the incorporation of lanthanum oxide.<sup>25</sup>

The porosity of the synthesized adsorbents was determined by measuring the N<sub>2</sub> adsorption–desorption isotherms at 77 K. Figure 2 shows the N<sub>2</sub> isotherms of porous carbon and La<sub>2</sub>O<sub>3</sub>/porous carbon, and the textural properties are presented in Table 1. Pristine porous carbon showed high adsorption of N<sub>2</sub> below the relative pressure P/P<sub>0</sub> = 0.1 and a hysteresis loop between the relative pressure of 0.4 and 1.0. As per the classification of porous materials by IUPAC, the isotherm of the porous carbon material is similar to type I and type IV isotherms.<sup>26</sup> This indicated that the synthesized porous carbon has micropores and mesopores. The specific surface area, pore volume and pore size of porous carbon were 826 m<sup>2</sup> g<sup>-1</sup>, 0.89 cm<sup>3</sup> g<sup>-1</sup> and 4.3 nm, respectively. Similarly, La<sub>2</sub>O<sub>3</sub>/porous carbon showed an isotherm curve similar to that of pristine porous carbon. However, the amount of N<sub>2</sub> adsorption was less, which

indicated that the pores of pristine porous carbon were occupied with lanthanum oxide. Hence, a change in the textural properties was observed. The specific surface area, pore volume and pore size of La<sub>2</sub>O<sub>3</sub>/porous carbon were 715 m<sup>2</sup> g<sup>-1</sup>, 0.76 cm<sup>3</sup> g<sup>-1</sup> and 4.2 nm, respectively. Lou et al.<sup>27</sup> have also observed a change in textural properties by the occupation of ruthenium nanoparticles within the pores of porous carbon material.

Morphological images with chemical composition for porous carbon and La<sub>2</sub>O<sub>3</sub>/porous carbon are shown in Figure 3. Disordered carbon particles were observed for porous carbon (Figure 3(a)). In La<sub>2</sub>O<sub>3</sub>/porous carbon, the loaded La<sub>2</sub>O<sub>3</sub> covers the surface of the disordered porous carbon (Figure 3(b)). From energy-dispersive X-ray (EDX) results, the amount of lanthanum was 2.97 wt%.

### Study of CO<sub>2</sub> and N<sub>2</sub> adsorption

The adsorption of CO<sub>2</sub> and N<sub>2</sub> has been studied by the volumetric method using porous carbon and La<sub>2</sub>O<sub>3</sub>/porous carbon. The CO<sub>2</sub> and N<sub>2</sub> adsorption isotherms are shown in Figure 4. CO<sub>2</sub> adsorption increased on increasing the pressure, but no equilibrium was attained for both adsorbents. The amount of CO<sub>2</sub> adsorption was 21 cm<sup>3</sup> g<sup>-1</sup> for porous carbon and 33 cm<sup>3</sup> g<sup>-1</sup> for La<sub>2</sub>O<sub>3</sub>/porous carbon at 298 K and 1 bar. The high adsorption of CO<sub>2</sub> with La<sub>2</sub>O<sub>3</sub>/porous

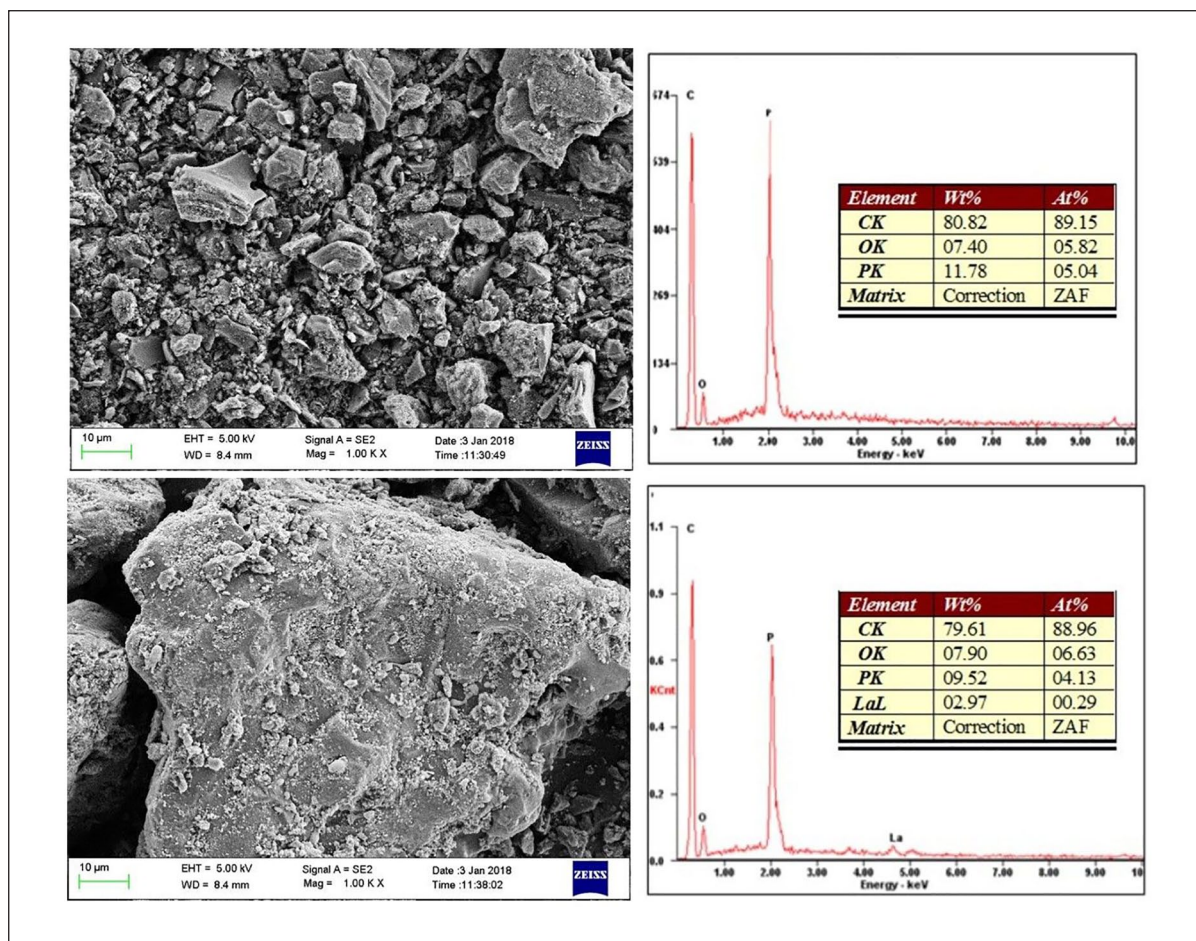


Figure 3. SEM with EDX images of (a) porous carbon and (b)  $\text{La}_2\text{O}_3$ /porous carbon.

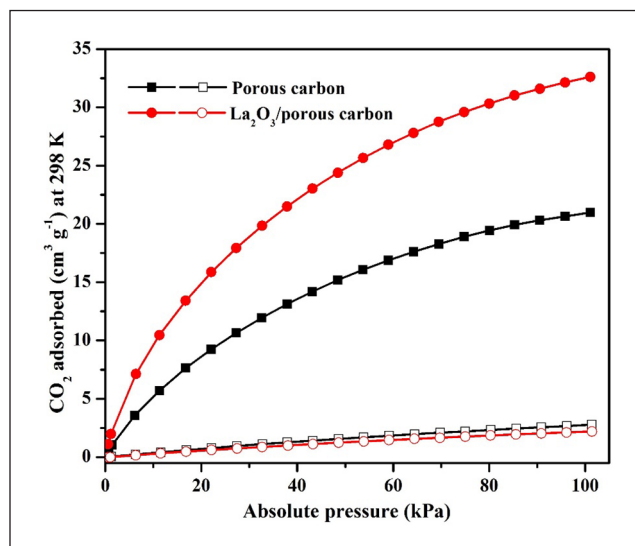


Figure 4.  $\text{CO}_2$  and  $\text{N}_2$  adsorption of porous carbon and  $\text{La}_2\text{O}_3$ /porous carbon (closed symbol:  $\text{CO}_2$  adsorption, open symbol:  $\text{N}_2$  adsorption).

carbon was due to the electrostatic interaction between lanthanum oxide and  $\text{CO}_2$ . Along with the  $\text{CO}_2$  adsorption study,  $\text{N}_2$  adsorption was also studied under similar conditions to those used for the  $\text{CO}_2$  adsorption study. The amount of  $\text{N}_2$  adsorption was  $2.8 \text{ cm}^3 \text{ g}^{-1}$  for porous carbon and  $2.2 \text{ cm}^3 \text{ g}^{-1}$  for  $\text{La}_2\text{O}_3$ /porous carbon at 298 K and 1 bar.

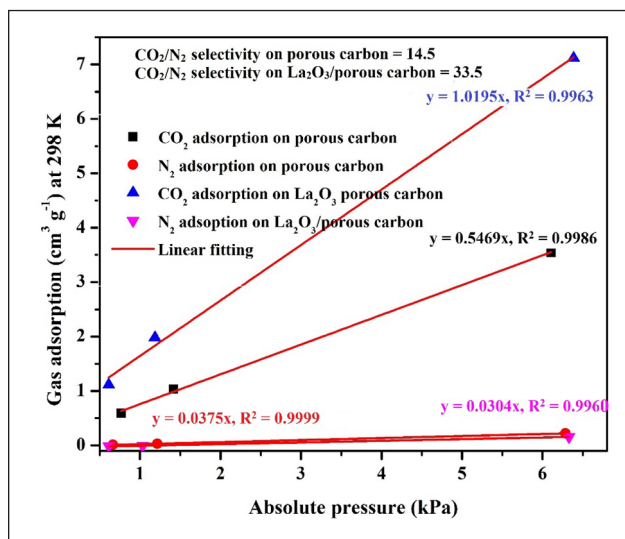
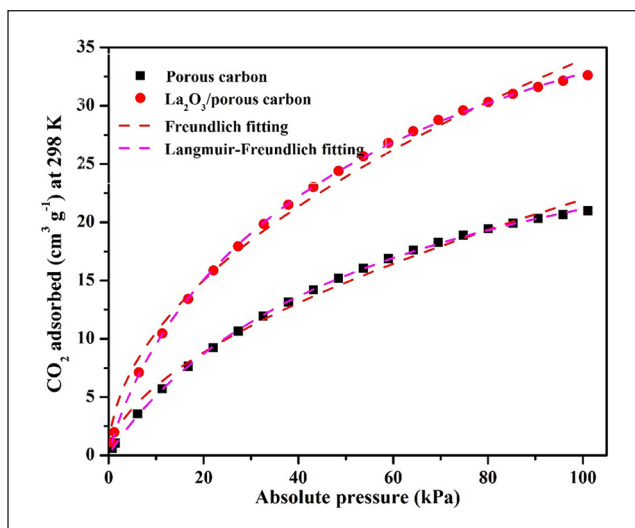


Figure 5.  $\text{CO}_2/\text{N}_2$  selectivity on porous carbon and  $\text{La}_2\text{O}_3$ /porous carbon.

The decrease in  $\text{N}_2$  adsorption was due to a change in the surface area.

In flue gas, carbon dioxide is a major component. So, it is essential to study  $\text{CO}_2/\text{N}_2$  selectivity. The initial slope method was used to calculate  $\text{CO}_2/\text{N}_2$  selectivity.<sup>28</sup> Figure 5 shows the  $\text{CO}_2/\text{N}_2$  selectivity with porous carbon and  $\text{La}_2\text{O}_3$ /porous carbon. For porous carbon, the





**Figure 6.** Fitting of isotherm models for CO<sub>2</sub> adsorption on porous carbon and La<sub>2</sub>O<sub>3</sub>/porous carbon.

CO<sub>2</sub>/N<sub>2</sub> selectivity was 14.5, whereas for La<sub>2</sub>O<sub>3</sub>/porous carbon, the selectivity was 33.5. High selectivity was obtained for La<sub>2</sub>O<sub>3</sub>/porous carbon because of the high adsorption of CO<sub>2</sub> and the selectivity value was higher than those of some reported adsorbents such as HKUST-1 and Mg-MOF-74.<sup>29,30</sup>

The adsorption behaviour of an adsorbent can be calculated by fitting of the experimental CO<sub>2</sub> adsorption with the Freundlich and Langmuir-Freundlich isotherm models.<sup>31</sup> The isotherm models can be written as follows

$$\text{Freundlich isotherm model : } Q = k_F P^{1/n}$$

$$\text{Langmuir - Freundlich isotherm model : } Q = \frac{Q_{\max} KP^{1/n}}{1 + KP^{1/n}}$$

where  $Q$  is the adsorption capacity at equilibrium (cm<sup>3</sup> g<sup>-1</sup>);  $Q_{\max}$  is the maximum adsorption capacity (cm<sup>3</sup> g<sup>-1</sup>);  $P$  is the pressure (kPa);  $k_F$  and  $K$  are the Freundlich and Langmuir-Freundlich constants, respectively; and  $n$  is the heterogeneity factor. The experimental CO<sub>2</sub> adsorption of porous carbon and La<sub>2</sub>O<sub>3</sub>/porous carbon are fitted with the Freundlich and Langmuir-Freundlich isotherm models, as shown in Figure 6. The fitting parameters are presented in Supplemental Table S1. The Langmuir-Freundlich isotherm model was well-fitted with the experimental CO<sub>2</sub> adsorption, regression co-efficient  $R^2 > 0.999$ . The  $Q_{\max}$  was higher for La<sub>2</sub>O<sub>3</sub>/porous carbon because of the strong interaction of CO<sub>2</sub> with lanthanum oxide.

In gas adsorption studies, the heat of adsorption ( $Q_{st}$ ) is an important parameter. It describes the interaction between the adsorbate and adsorbent. The  $Q_{st}$  can be calculated using the virial equation<sup>32</sup>

$$\text{Virial equation : } \ln P = \ln N + \frac{1}{T} \sum_{i=0}^m a_i N^i + \sum_{j=0}^n b_j N^j$$

$$\text{Heat of adsorption : } Q_{st} = -R \sum_{i=0}^m a_i N^i$$

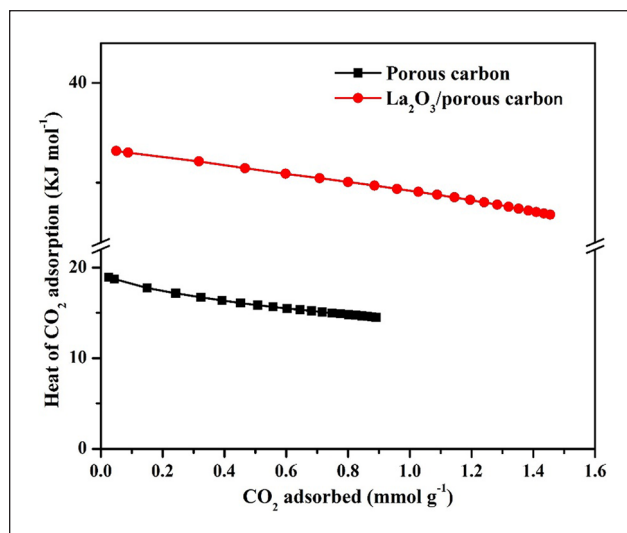


**Figure 7.** The heat of CO<sub>2</sub> adsorption of porous carbon and La<sub>2</sub>O<sub>3</sub>/porous carbon.

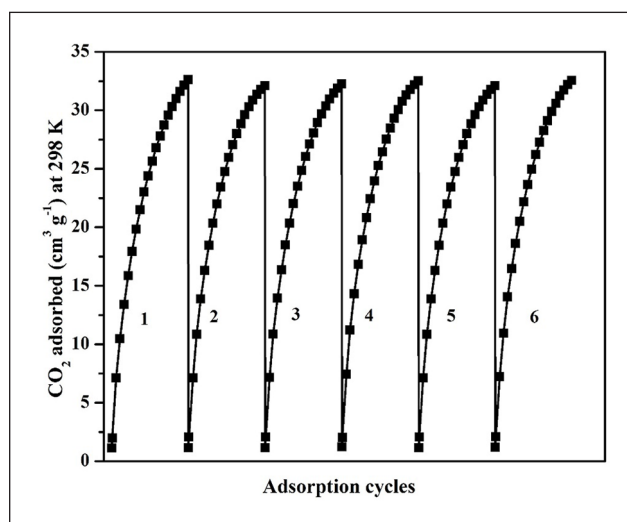


**Figure 8.** Multiple CO<sub>2</sub> adsorption cycles of La<sub>2</sub>O<sub>3</sub>/porous carbon.

where  $P$  is the pressure in Torr,  $N$  is the gas uptake in cm<sup>3</sup> g<sup>-1</sup>,  $T$  is the temperature in K,  $R$  is the universal gas constant (8.314 JK<sup>-1</sup> mol<sup>-1</sup>),  $Q_{st}$  is the heat of adsorption in kJ mol<sup>-1</sup>,  $a_i$  and  $b_j$  are the virial coefficients, and  $m$  and  $n$  are the number of coefficients. To calculate the heat of CO<sub>2</sub> adsorption for porous carbon and La<sub>2</sub>O<sub>3</sub>/porous carbon, CO<sub>2</sub> adsorption at 303 K was measured for both samples (see Supplemental Figure S1). The amount of CO<sub>2</sub> adsorption was less at 303 K compared with CO<sub>2</sub> adsorption at 298 K because of the increase in the kinetic energy of CO<sub>2</sub>. The measured CO<sub>2</sub> adsorption isotherms were fitted with the virial equation (Supplemental Figure S2). From the virial fitting parameters, the heat of CO<sub>2</sub> was calculated. The heat of CO<sub>2</sub> adsorption of porous carbon and La<sub>2</sub>O<sub>3</sub>/porous carbon is shown in Figure 7. For porous carbon,  $Q_{st}$  was 18.9–14.5 kJ mol<sup>-1</sup>, whereas for La<sub>2</sub>O<sub>3</sub>/porous carbon was 36.5–33.4 kJ mol<sup>-1</sup>. A high  $Q_{st}$  was obtained for La<sub>2</sub>O<sub>3</sub>/porous carbon because of the strong interaction between CO<sub>2</sub> and lanthanum oxide. At



**Table 2.** Comparison of the CO<sub>2</sub> adsorption capacity of La<sub>2</sub>O<sub>3</sub>/porous carbon with reported adsorbents.

Sample	Adsorption method	CO <sub>2</sub> adsorbed (cm <sup>3</sup> g <sup>-1</sup> ) at 298 K, 1 bar	Reference
ZIF-98	Volumetric	34	Wang et al. <sup>33</sup>
S-doped microporous carbon	Volumetric	54	Xia et al. <sup>34</sup>
N-doped microporous carbon	Volumetric	53.7	An et al. <sup>35</sup>
Mesoporous N-doped CeO <sub>2</sub>	Gravimetric	24 (303 K)	Wang et al. <sup>36</sup>
PEHA-MIL-101	Volumetric	29	Anbia et al. <sup>37</sup>
Zeolite-13X	Volumetric	38	McEwen et al. <sup>38</sup>
La <sub>2</sub> O <sub>3</sub> /porous carbon	Volumetric	33	Present work

low adsorption of CO<sub>2</sub>, a high Q<sub>st</sub> was obtained. With an increase in CO<sub>2</sub> adsorption, the Q<sub>st</sub> decreased due to a decrease in the number of active adsorption sites.

Multiple CO<sub>2</sub> adsorption cycles have been studied to determine the adsorption stability of La<sub>2</sub>O<sub>3</sub>/porous carbon at 298 K (Figure 8). Before studying the CO<sub>2</sub> adsorption cycle, the adsorbent was degasified at 473 K for 2 h under vacuum to remove the adsorbed CO<sub>2</sub>. The amount of CO<sub>2</sub> adsorption was constant in each adsorption cycle. The CO<sub>2</sub> adsorption of La<sub>2</sub>O<sub>3</sub>/porous carbon was compared with the CO<sub>2</sub> adsorption capacity of previously reported adsorbents (Table 2). The synthesized La<sub>2</sub>O<sub>3</sub>/porous carbon showed 33 cm<sup>3</sup>g<sup>-1</sup> of CO<sub>2</sub> adsorption at 298 K and 1 bar, which was in-between the CO<sub>2</sub> adsorption capacity of mesoporous N-doped CeO<sub>2</sub> and S-doped microporous carbon.<sup>34,36</sup>

## Conclusion

In this work, we have studied CO<sub>2</sub> adsorption and separation by the volumetric method using porous carbon and La<sub>2</sub>O<sub>3</sub>/porous carbon. The high CO<sub>2</sub> adsorption capacity was obtained on La<sub>2</sub>O<sub>3</sub>/porous carbon compared to bulk porous carbon at 298 K and 1 bar because of electrostatic interaction of La<sub>2</sub>O<sub>3</sub> with CO<sub>2</sub> and CO<sub>2</sub>/N<sub>2</sub> selectivity was also higher on La<sub>2</sub>O<sub>3</sub>/porous carbon. The heat of CO<sub>2</sub> adsorption was 36.5 kJmol<sup>-1</sup> at low coverage of CO<sub>2</sub> for La<sub>2</sub>O<sub>3</sub>/porous carbon and CO<sub>2</sub> adsorption capacity was constant in each adsorption cycle. Therefore, a basic metal oxide can be incorporated on porous carbon to increase the CO<sub>2</sub> adsorption and separation.

## Experimental

Lanthanum nitrate hexahydrate [La(NO<sub>3</sub>)<sub>3</sub>·6H<sub>2</sub>O, 99.9%] and orthophosphoric acid (H<sub>3</sub>PO<sub>4</sub>, 85%) were purchased from Sigma-Aldrich, India, and used without purification. Distilled water was used to synthesize the adsorbents. High purity gases (carbon dioxide, nitrogen and helium) were purchased from BOC, India.

Porous carbon was synthesized by using pongamia pinata fruit hulls which were collected from the forest region of Telangana, India. First, the fruit hulls were washed, dried then made into a powder. The powder was activated using phosphoric acid at room temperature for 24 h followed by drying at 373 K for 12 h. The dried sample was calcined under nitrogen gas with a flow rate of 50 mL/min at 723 K for 4 h, with a heating rate of 5 K/min, and then cooled to room temperature. The sample was washed with distilled water until the pH

reached 7, then it was dried at 373 K overnight to afford porous carbon.<sup>39</sup> Porous carbon supported lanthanum oxide was synthesized by the impregnation method.<sup>40</sup> About 0.1 g of lanthanum nitrate hexahydrate was dissolved in 10 mL of distilled water, stirred for 10 min then 1 g of porous carbon was added. The mixture was stirred at room temperature for 1 h and then dried at 373 K overnight. The dried compound was calcined under nitrogen gas at 873 K for 3 h.

XRD patterns were recorded on a Rigaku Ultima-IV X-ray diffractometer using Ni-filtered Cu-K<sub>α</sub> radiation operated at a voltage of 40 kV and a current of 30 mA in the scan range of 2θ = 10°–80° with a step size of 0.02°/s. A Micrometric ASAP 2020 porosity analyzer was used to measure N<sub>2</sub> adsorption–desorption isotherms at 77 K. Prior to the adsorption study, about 0.1 g of the sample was degassed at 473 K for 2 h under vacuum. The multi-point Brunauer–Emmett–Teller (BET) surface area was calculated in the relative pressure range of 0.05–0.3, the total pore volume at a relative pressure of 0.99, the micropore volume by the t-plot method and the mesopore volume was calculated by subtracting the micropore volume from the total pore volume. The pore size distribution was plotted using non-local density functional theory. A LabRAM HR800 spectrometer was used to record the Raman spectra. The morphology and elemental composition of each sample were determined from scanning electron microscopy with energy-dispersive X-ray (SEM with EDX) analysis using a ZEISS Sigma 300 scanning electron microscopy analyzer.

The adsorption of CO<sub>2</sub> and N<sub>2</sub> was carried out using a Micromeritics ASAP 2020 gas adsorption analyzer at low pressure and at 298 K. A thermostatic bath connected with water circulating jacket was used to control the sample temperature, and helium gas was used to determine the free space of the sample tube. Before the gas adsorption measurement, 0.1 g of the sample was activated at 473 K for 2 h under vacuum to remove moisture or adsorbed gases and then cooled to the gas adsorption temperature. Ultra-high pure gases were used to measure the adsorption isotherms. The initial slope method was used to calculate the selectivity of CO<sub>2</sub>/N<sub>2</sub>. The virial method was used to calculate the heat of CO<sub>2</sub> adsorption using adsorption isotherms obtained at 298 and 303 K. The CO<sub>2</sub> adsorption cycles were also studied at 298 K to calculate the adsorption stability of an adsorbent.

## Declaration of conflicting interests

The author(s) declared no potential conflicts of interest with respect to the research, authorship and/or publication of this article.

## Funding

The author(s) disclosed receipt of the following financial support for the research, authorship and/or publication of this article: The authors acknowledge the Science and Engineering Research Board, Department of Science and Technology, New Delhi, India, for financial support (grant no. EMEQ-283/2014).

## ORCID iD

Madhavi Jonnalagadda  <https://orcid.org/0000-0003-2429-2493>

## Supplemental material

Supplemental material for this article is available online.

## References

1. Hosseini S, Bayesti I, Marahel E, et al. *J Taiwan Inst Chem Eng* 2015; 52: 109.
2. Zhang XQ, Li WC and Lu AH. *New Carbon Mater* 2015; 30: 481.
3. Sarker AI, Aroonwilas A and Veawab A. *Energy Procedia* 2017; 114: 2450.
4. Sanz-Pérez ES, Arencibia A, Calleja G, et al. *Microporous and Mesoporous Mater* 2018; 260: 235.
5. Zhang H, Yan Y and Yang L. *Adsorption* 2010; 16: 161.
6. Heo YJ and Park SJ. *J Ind Eng Chem* 2015; 31: 330.
7. Gurten II, Ozmak M, Yagmur E, et al. *Biomass Bioenergy* 2012; 37: 73.
8. Foo KY and Hameed BH. *Bioresor Technol* 2013; 130: 696.
9. Deng H, Zhang G, Xu X, et al. *J Hazard Mater* 2010; 182: 217.
10. Alslaibi TM, Abustan I, Ahmad MA, et al. *J Dispersion Sci Technol* 2014; 35: 913.
11. Torrellas SA, García Lovera R, Escalona N, et al. *Chem Eng J* 2015; 279: 788.
12. Khanday WA, Marrakchi F, Asif M, et al. *J Taiwan Inst Chem Eng* 2017; 70: 32.
13. Laksaci H, Khelifi A, Trari M, et al. *J Clean Prod* 2017; 147: 254.
14. Liu S, Ma R, Hu X, et al. *Ind Eng Chem Res* 2020; 59: 7046.
15. Yue L, Rao L, Wang L, et al. *Energy Fuel* 2018; 32: 6955.
16. Yang P, Rao L, Zhu W, et al. *Ind Eng Chem Res* 2020; 59: 6194.
17. Bhagiyalakshmi M, Hemalatha P, Ganesh M, et al. *Fuel* 2011; 90: 1662.
18. Li M, Huang K, Schott JA, et al. *Microporous Mesoporous Mater* 2017; 249: 34.
19. Kim BJ, Cho KS and Park SJ. *J Colloid Interface Sci* 2010; 342: 575.
20. Jang DI and Park SJ. *Fuel* 2012; 102: 439.
21. Burri H, Anjum R, Gurram RB, et al. *Korean J Chem Eng* 2019; 36: 1482.
22. Shang H, Lu Y, Zhao F, et al. *RSC Adv* 2015; 5: 75728.
23. Chanapattathapol KC, Krachumram S and Youngme S. *Microporous Mesoporous Mater* 2017; 245: 8.
24. Sogut EG, Acidereli H, Kuyuldar E, et al. *Sci Rep* 2019; 9: 15724.
25. Cheng S, Zhang L, Xia H, et al. *Journal* 2017; 6: 487.
26. Brunauer S, Emmett PH and Teller E. *J Am Chem Soc* 1938; 60: 309.
27. Lou BS, Veerakumar P, Chen SM, et al. *Sci Rep* 2016; 6: 19949.
28. Khutia A. *Dalton trans* 2013; 43.
29. Montoro C, García E, Calero S, et al. *J Mater Chem* 2012; 22: 10155.
30. Britt D, Furukawa H, Wang B, et al. *Pro Natl Acad Sci USA* 2009; 106: 20637.
31. Mutyala S, Yakout SM, Ibrahim SS, et al. *New J Chem* 2019; 43: 9725.
32. Moon HS, Moon JH, Chun DH, et al. *Microporous Mesoporous Mater* 2016; 232: 161.
33. Wang B, Côté AP, Furukawa H, et al. *Nature* 2008; 453: 207.
34. Xia Y, Zhu Y and Tang Y. *Carbon* 2012; 50: 5543.
35. An L, Liu S, Wang L, et al. *Ind Eng Chem Res* 2019; 58: 3349.
36. Wang Y, Yin C, Qin H, et al. *Dalton Trans* 2015; 44: 18718.
37. Anbia M and Hoseini V. *J Nat Gas Chem* 2012; 21: 339.
38. McEwen J, Hayman JD and Ozgur Yazaydin A. *Chem Phys* 2013; 412: 72.
39. Islam MA, Sabar S, Benhouria A, et al. *J Taiwan Inst Chem Eng* 2017; 74: 96.
40. Mutyala S, Yu YD, Jin WG, et al. *J Porous Mater* 2019; 26: 1831.



A/c Dy No: 66  
Date: 11/06/18

UNIVERSITY GRANTS COMMISSION-SOUTH EASTERN REGIONAL OFFICE  
5-9-194, CHIRAG ALI LANE, IV FLOOR A.P.S.F.C. BUILDING, HYDERABAD -500 001  
Phones: 040 - 23204735, 23200208 FAX: 040 - 23204734, Website: www.ugc.ac.in,ugcsero@gmail.com

No: F. MRP-6327/15 GEN/( UGC-SERO)

June, 2018

The Accounts Officer  
South Eastern Regional Office  
University Grants Commission  
Hyderabad - 500 001

LINKNO:6327. DEPT:BOTANY  
COMCODE: APKA018

UniqueID: TLKA00000643

11/06/18 20:0

Sub: Release of Grants-in-aid to The Principal GOVT. DEGREE COLLEGE FOR WOMEN, KARIMNAGAR KARIMNAGAR DIST. 505001. Under the Scheme "Minor Research Projects" - Reg.

Sir/Madam,

On the basis of the accounts received for the grants released earlier under the scheme, I am to convey the sanction of the Commission for the payment of Rs.90000. to The Principal, GOVT. DEGREE COLLEGE FOR WOMEN, KARIMNAGAR KARIMNAGAR DIST. 505001. as final instalment towards the Minor Research Project entitled IN VITRO MICROPROPAGATION OF GYMNEMA SYL TZ) R. BR. EX ROEMER & SCHULTES. AN IMPO CINAL PLANT. submitted by DR. UPPU ANITHA DEVI Department of BOTANY as per the details given below:-

Item	Allocation (Rs.)	Amount already released (Rs.)	Amount sanctioned now (Rs.)	Total grant sanctioned/released so far (Rs.)
Hiring Services	00	00	00	00
Contingency	50000.	25000.	25000.	50000.
Chemicals	90000.	45000.	45000.	90000.
Travel/Field Work	40000.	20000.	20000.	40000.
Total	180000.	90000.	90000.	180000.
Equipment	100000.	100000.	00	100000.
Books	20000.	20000.	00	20000.
Total	120000.	120000.	00	120000.
Grand Total	300000.	210000.	90000.	300000.

1. The grant is debitible to following head of account.

Amount Sanctioned	Head Of Accounts	Category
Rs.90000	31-GIA-MRP(50)-3(A)2202.03.102.02.01	GEN

2. The sanctioned amount is debitible to the Head of Account 31-GIA-MRP(50)-3(A)-2202.03.102.02.01 (General) and is valid for payment during the financial year 2018-19 Only and the amount of the Grant shall be drawn by the Accounts Officer (Drawing and Disbursing Officer) UGC-SERO, Hyd. on the Grants-In Aid Bill and shall be disbursed to and credited to "The Principal, GOVT. DEGREE COLLEGE FOR WOMEN, KARIMNAGAR, KARIMNAGAR DIST. by Electronic Mode through PFMS Portal at the following details: "(a) Name & Address of Account Holder: The Principal, GOVT. DEGREE COLLEGE FOR WOMEN, KARIMNAGAR, KARIMNAGAR DIST. (b) Name & Address of Bank Branch: IOB, KARIMNAGAR

(c) Account No: 040501000016201 (d) IFSC Code: IOBA0000405.

- The Grant is subject to the adjust on the basis of Utilization Certificate in the prescribed Proforma submitted by the Institution.
- The Institution shall maintain proper accounts of the expenditure out of the Grants which shall be utilized only on the approved items of expenditure.
- The institution may follow the General Financial Rules, 2017 and take urgent necessary action to amend their manuals of financial procedures to bring them in conformity with GFRs, 2005 and those don't have their own approved manuals on financial procedures may adopt the provision of GFRs 2005 and instructions / Guidelines there under from time to time.
- The Utilization Certificate to the effect that the grant has been utilized for the propose for which it has been sanctioned shall be furnished to UGC as early as possible after the close of current financial year.
- The assets acquired wholly or substantially out of UGC's Gant shall NOT be disposed or encumbered or utilized for the proposes other than those for which the grant was given without proper sanction of the UGC and should at any time the Institution ceased to function, such assets shall revert to the University Grants Commission.
- A Register of Assets acquired wholly or substantially out of the Grant shall be maintained by the Institution in the prescribed proforma.
- The Grantee Institution shall ensure the utilization of Grants-in-Aid for the purpose for which it is being sanctioned / paid. In case of Non-Utilization / Part Utilization thereof, simple interest @ 10% per annum, as amended from time to time on the unutilized amount from the date of credit of amount to the date of refund as per provision contained in General Financial Rules of Govt. of India will be charged.

P.T.O.